Measurement report: Intra/interannual variability and source apportionment of VOCs during 2018–2020 in Zhengzhou, Central China

Shijie Yu [a,b], Shenbo Wang[b,c], Ruixin Xu [b,c], Dong Zhang [a,b], Meng Zhang [e], Fangcheng Su[b,c], Xuan Lu[a,b], Xiao Li[b,c], Ruiqin Zhang [b,c]*, Lingling Wang [d]*

a. College of Chemistry, Zhengzhou University, Zhengzhou 450001, China

b. Institute of Environmental Sciences, Zhengzhou University, Zhengzhou 450001, China

c. School of Ecology and Environment, Zhengzhou University, Zhengzhou 450001, China

d. Environmental Monitoring Center of Henan Province，Zhengzhou 450000

e. Pingdingshan Ecological Environment Monitoring Center of Henan Province, Pingdingshan 467000, China

*Correspondence author. Research Institute of Environmental Science, College of Environment and Ecology, Zhengzhou University High-tech Development Zone, Zhengzhou, Henan, PR China, 450001

E-mail address: rqzhang@zzu.edu.cn

Abstract:

Ambient volatile organic compounds (VOCs) were measured continuously from January 2018 to December 2020 at an urban site in Zhengzhou (China) to investigate their characteristics, sources, atmospheric oxidation capacity (AOC), and chemical reactivity. During the sampling period, the total concentration of observed VOCs was 94.3±53.1 μg/m^3 ppbv and alkanes were the major VOC species, accounting for 58% of the total. During the sampling period, the interannual variation of VOCs gradually reduced from 113.2±65.2 μg/m^3 in 2018, 90.7±52.5 μg/m^3 in 2019, and 79.1±41.7 μg/m^3 in 2020. Ethane and propane were the top two most abundant species during the three-year observation period. Results showed that the total AOC, dominated by OH radical reactions, was 7.4 × 10^7 molecules cm^{-3} s^{-1}. Total OH reactivity was 45.3 s^{-1} and it was mainly contributed by NOx. The AOC and •OH reactivity both exhibited well-defined seasonal and interannual patterns. Therefore, control strategies should focus on the key species given their interannual and seasonal variations. Meanwhile, diagnostic ratios of VOC species indicated that VOCs in Zhengzhou were greatly affected by vehicle emissions and liquid petroleum gas/natural gas (LPG/NG). Positive matrix factorization analysis identified six sources: industrial sources, solvent use, vehicle emissions, LPG/NG, fuel burning, and biogenic sources. Vehicle emissions and industrial sources made the largest contributions to VOC emission in each of the three years. The proportion of the contributions of vehicle emissions and LPG/NG increased with each passing year. However, the proportion of industrial and solvent sources presented a decreasing trend, which reflects the remarkable effect of control policies. The effect of VOCs on O_3 formation suggests that vehicle emissions and solvent use remain key sources. Therefore, it is necessary to formulate effective strategies for reducing ground-level O_3, and those sources mentioned above should be strictly controlled by the regulatory authorities.

1. Introduction

In recent years, regional atmospheric pollution events have occurred frequently

around the world, with many areas suffering severe haze episodes in autumn and winter, and O_3 pollution in summer (Uttamang et al., 2020; Li et al., 2019; Sadeghi et al., 2021; Yan et al., 2018; Yadav et al., 2019; Zhang et al., 2018). Volatile organic compounds (VOCs) are important precursors of secondary pollutants such as O_3 and secondary organic aerosols, and the study of VOCs is a primary focus among the scientific community and relevant governing bodies (Liu et al., 2019a; Song. et al., 2019c; Xu et al., 2017).

VOCs encompass a large variety of species, and the chemical reactivity of each species varies greatly. Thus, elucidation of VOC characteristics and active substance identification represent research priorities. In many regions, alkanes represent the dominant VOC species, while studies which do not report OVOCs usually identify aromatics and alkenes as better contributors of ozone formation potential (OFP) (Li et al., 2019b; Yan et al., 2017). Following a study in Wuhan (China), Yang et al. (2019) suggested that alkanes were the dominant group, accounting for 42% of the total VOC concentration, and that C_2-C_3 hydrocarbons were the dominant active substance. Huang and Hsieh (2019) studied the maximum incremental reactivity (MIR) and propylene-equivalent (PE) concentration, reporting that toluene was the largest potential contributor to the OFP and that industrial emissions contributed nearly 60% to the OFP. Given the complex composition of VOCs in the atmosphere, it is difficult to determine the sources of VOCs. To apportion the source contributions of VOCs, it is common practice to use receptor models that include positive matrix factorization (PMF), chemical mass balance, and principal component analysis. In China, traffic emissions are often the main source of VOCs, particularly in major metropolitan areas (Li et al., 2019; Liu et al., 2019; Song, et al., 2019b). Moreover, industrial processes and solvent use have remarkable influence on VOC emissions (Hui et al., 2019; Mo et al., 2017). Biogenic sources also cannot be ignored owing to their high reactivity, which can contribute 5%–20% of VOC emissions (Wu et al., 2016). In addition to the study of VOC characteristics and source apportionment, analysis of atmospheric oxidation characteristics is another area of hot topic. Variations in the atmospheric oxidation capacity (AOC) not only affect the O_3 level in summer but also greatly

impact the generation of secondary particles throughout the entire year (Prinn, 2003). However, most previous related studies in China focused on metropolitan areas such as the Beijing–Tianjin–Hebei region (Gu et al., 2019b), Pearl River Delta region (Zhang et al., 2015), and Yangtze River Delta region (Xu et al., 2017; Zheng et al., 2020), while less research has been conducted in heavily polluted areas of the central plains. Moreover, previous studies frequently used short-term monitoring data that cannot fully reflect the comprehensive VOC pollution characteristics within a region. Therefore, it is an urgent requirement that large-scale investigations be conducted on the central plains of China.

As the political and cultural center of Henan Province, Zhengzhou had more than 10 million permanent residents and 4.0 million private vehicles in 2019 (Gu et al., 2019a). This area is often confronted with severe haze episodes and photochemical pollution due to emission of huge amounts of air pollutants (Li et al., 2020b). Consequently, much research has been conducted on air pollution in Zhengzhou, but many of the earlier studies focused only on particulate matter (Jiang et al., 2018; Wang et al., 2019). Few studies have addressed VOCs in Zhengzhou, especially in relation to longer sampling periods and seasonal measurements. Following adjustment of control policies and optimization of the energy structure, recent mitigation measures might have affected the characteristics and sources of VOCs. Therefore, it is necessary to identify local VOC pollution characteristics on the basis of a long time series of monitoring data, which could provide a reference for formulation of local air pollution control measures.

To deepen the understanding of VOC pollution characteristics, chemical reactivity, and source contribution, VOC data were measured in Zhengzhou using online instruments from 2018–2020. The aims of this research were as follows: (1) analyze the characteristics of VOC variation in Zhengzhou, including diurnal, seasonal, and annual changes; (2) quantify the contribution of sources among intra/interannual variations and identify the locations of VOC sources; (3) parameterize the AOC and speciate OH reactivity; and (4) assess O_3 formation by MIR and PE analysis.

2. Methodology

2.1 Study site and measurements

The observation period of this study was from January 2018 to December 2020. The VOC samples were collected at an urban site (34°45′N, 113°41′E) by the Department of Environmental Protection of Henan Province. The surrounding environment represents a typical urban environment in Zhengzhou, comprising commercial and residential districts with traffic sources (Fig. 1).

The VOC species were monitored continuously using an auto-GC system with a 1-h time resolution (AMA Instruments GmbH, Germany). Specific information regarding this system is described in Zou et al. (2015). The 57 VOC species (comprising 29 alkanes, 10 alkenes, 1 alkyne, and 17 aromatics) were calibrated using the VOC Standards of the U.S. EPA PAMS mixture (Spectra Gases, USA) before monitoring. During the observation period, zero and span gas checks (PAMS calibration gases) were conducted monthly using the 5-point method, together with adjustment of the retention time. Data quality control of this instrument is detailed in our previous study (Ren et al., 2020). Overall, the correlation coefficient varied from 0.990–0.999, and the detection limits were in the range of 0.02–0.12 ppbv, as shown in Table S1.

Meteorological data comprising atmospheric temperature (T), relative humidity, ultraviolet (UV) radiation, precipitation (Pr), planetary boundary layer height, wind speed (WS), and wind direction (WD) were obtained from the surface meteorological station of the Henan monitoring center. Datasets of trace gases such as the hourly concentrations of NO, NO_2, CO, O_3, SO_2, and fine particles ($PM_{2.5}$) were obtained from the ambient air quality observation station of Yanchang, which is located approximately 2 km from the VOC monitoring station.

2.2 Positive matrix factorization (PMF) model

In this study, analysis of the source of the VOCs was performed using the EPA

PMF 5.0 model, which is a receptor model used widely for source apportionment (Gao et al., 2018; Yadav et al., 2019). Detailed information regarding this method is available in the user manual (Norris et al., 2014) and other related literature (Song et al., 2019a, 2019b). Two input files are required for PMF: the concentration values and the uncertainty values of the individual VOC species. The uncertainty is calculated using Eq. (1) when the species concentration value is higher than its method detection limit (MDL), or using Eq. (2) when the concentration is less than or equal to the MDL:

$$\mathrm{Unc} = \sqrt{(\mathrm{EF} \times c)^2 + (0.5 \times \mathrm{MDL})^2}, \quad (1)$$

$$\mathrm{Unc} = {}^{5}/_{6} \times \mathrm{MDL}, \quad (2)$$

where c is the concentration of the individual VOC species, and EF is the error fraction, which was set to 10% of the VOC concentration (Yuan et al., 2012).

Owing to the complexity of the chemical reactions, not all of the VOC species were used in the PMF analysis. Based on previous work, this study adopted the following principles for selection of the VOC species. (1) Species with more than 25% of data missing or below the MDLs were rejected, which follows the methodology of previous studies (Zhou et al., 2019). (2) Species with short atmospheric lifetimes were excluded because they rapidly react away in the atmosphere. (3) Species that represent source tracers of emission sources were retained (e.g., in the case of isoprene). Eventually, 27 VOC species were selected for source apportionment analysis. VOC species were grouped into strong, weak and bad according to their signal/noise ratio (S/N), and there were 23 and 4 species grouped into strong and weak, respectively. It should be noted that the volumetric concentration (ppbv) of the individual VOC species was converted to mass concentration (μg m^{-3}) before being input into the PMF model.

Choosing the optimal number of factors in the model is important. The number of factors depends on Q (ture)/Q (robust) and Q/Qexpected (Qexp). In theory, Q (ture)/Q (robust) < 1.5 and a value close to 1 is considered reasonable (Ulbrich et al., 2009), and the rate of change of Q/Qexp should be stable and the ratio should be close

to 1 (Baudic et al., 2016; Hui et al., 2019). In this study, the numbers of factors used for the PMF analysis were tested from three to eight, and the optimum six-factor solution with Q/Qexp = 0.94, (Q (ture)/Q (robust) = 1.0) was selected. Additionally, Fpeak values from −1 to 1 with 0.1 intervals were used in the model, and Fpeak = -0.2 was established as the best solution (as shown in Fig. S1).

2.3 Relative reactivity of VOCs

To better understand the role of VOCs in the formation of tropospheric O_3, the OFP and the PE concentration were investigated to analyze the chemical reactivity of the VOC species (Carter, 1994; Atkinson and Arey, 2003), and the detailed operation is described in the supplementary materials (Text S1).

2.4 Atmospheric oxidation capacity (AOC) and speciated oxidant reactivity

The AOC is defined as the sum of the respective oxidation rates of the primary pollutants (e.g., CO, CH_4, and VOCs) by the oxidants (e.g., OH, NO_3, and O_3), and it can be calculated using Eq. (3) (Elshorbany et al., 2009; Xue et al., 2016):

$$\mathrm{AOC} = \sum_i k_{Yi}[X][Y_i], \quad (3)$$

where $[X]$ and $[Y_i]$ are the number concentrations of molecule oxidant X and Y_i, respectively, and k_{Yi} is the bimolecular rate constant of molecule Y_i with oxidant X (Zhu et al., 2020). In this study, the reduced substances only included 57 PAMS (provided by Spectra Gases Inc., USA) and CO. The oxidants only included •OH, NO_3, and O_3 radicals. The concentration OH and NO_3 radicals was estimated from parameterization methods via Eqs. (4) and (5) (Carter, 1994; Warneke, 2004):

$$[\mathrm{OH}] = a \times (J_{O^1D})^{\alpha} \times (J_{NO_2})^{\beta} \times \frac{b\times[NO_2]+1}{c\times[NO_2]^2+d\times[NO_2]+1}, \quad (4)$$

where J_{O1D} and J_{NO2} are the measured photolysis frequency (s^{-1}) of O_3 and NO_2, respectively. The values of a, b, c, α, and β are 4.1×10^9, 140, 0.41, 1.7, 0.83, and 0.19, respectively (Yang et al., 2019).

NO_3 concentration in the atmosphere is based on the steady-state assumption (Liebmann et al., 2018):

$$[NO_3] = \frac{k_{NO_2} \times [NO_2] \times [O_3]}{J_{NO_3} + J_{NO+NO_3} \times [NO] + \sum_i k_{NO_3+VOC_i} \times [VOC]_i}, \quad (5)$$

where J_{NO3} is the measured photolysis frequency (s^{-1}) of NO_3. The rate coefficients for NO_2-O_3 (k_{NO2+O3}) and NO-NO_3 (k_{NO+NO3}) were obtained from Atkinson et al. (2004). Detailed descriptions of the calculation processes of OH and NO_3 are available in Yang et al. (2021).

Additionally, OH reactivity is another indicator of atmospheric oxidation. It is the inverse of the OH lifetime, and it can be defined as the product of the rate coefficients and the concentrations of the reactants with OH. Thus, OH reactivity can be calculated using Eq. (6) (Mao et al., 2010):

$$\text{OH reactivity} = \sum k_{OH+VOC_i} \times [VOC_i] + k_{OH+CO} \times [CO] + k_{OH+NO} \times [NO] + k_{OH+NO_2} \times [NO_2] + k_{OH+SO_2} \times [SO_2] + k_{OH+O_3} \times [O_3] + k_{OH+other} \times [other], \quad (6)$$

where *[Xi]* is the concentration of the species (e.g., CO, NOx, SO_2, and VOCs), and the rate coefficient k_{OH} (unit: cm^3 molecule1 s^{-1}) represents the corresponding reaction rate coefficient.

2.5 Conditional probability function (CPF) analysis

The conditional probability function (CPF) was developed to identify potential source contributions using the PMF source contribution solution, coupled with WD (Guo et al., 2011; Hsu et al., 2018; Wu et al., 2016). The CPF is defined as follows:

$$CPF = \frac{m_{\triangle\theta}}{n_{\triangle\theta}}, \quad (7)$$

where $m_{\triangle\theta}$ is the number of appearances from wind sector $\triangle\theta$ (each sector is 22.5°) that exceed the concentration threshold (75th percentile of each source contribution), and $n_{\triangle\theta}$ is the total number of occurrences in the same wind sector. Weak winds (WS < 1.5 m s^{-1}) were excluded from the calculation because of the difficulty in defining WD (Zheng et al., 2018).

3. Results and discussion

3.1 Characteristics of VOCs in Zhengzhou

3.1.1 Concentrations and compositions of VOCs

The average ambient VOC concentrations and chemical species measured in Zhengzhou during the study period are shown in Table S2. And Table S3 presented the comparison of VOCs between this study and other studies. The annual average concentration of VOCs was 94.3±53.1 μg/m^3 (38.2±15.6 ppbv), i.e., close to the concentration reported in Langfang (33.4 ppbv) (Song et al., 2019a) and Nanjing (34.4 ppbv) (Shao, et al. 2016), lower than that found in Chengdu (41.8 ppbv) (Song et al. 2018), Guangzhou (42.7 ppbv) (Zou et al., 2015), and higher than that reported in Tianjin (28.7 ppbv) (Liu et al. 2016). Among the observed species, alkanes were the major component of the VOCs with mean concentration of 54.7±37.9 μg/m^3, accounting for 58% of the total, followed by aromatics (25%), alkenes (13%) and alkynes (3%). Many previous related studies also reported that alkanes represent the dominant group (Fu et al., 2020; Gu et al., 2020), similar to the situation found in Zhengzhou. For the record, OVOCs were not simultaneously measured in this study due to the limitations on available instrumentation. Thus, those investigations apply only to studies which failed to measure OVOCs.

To clarify the characteristics of VOC emission sources, the concentrations of the 20 most abundant species, accounting for 83% of the compound classes monitored in the present study, are listed in Table 1. During the sampling period (2018–2020), the most important VOC species in Zhengzhou were ethane (11.7±6.8 μg/m^3), propane (8.2±4.9μg/m^3), toluene (6.5±4.5μg/m^3), i-pentane (6.1±10.4 μg/m^3), n-butane(5.8±4.1μg/m^3) and ethene (5.6±5.3μg/m^3). Generally, C_2-C_5 species are closely related to vehicular emissions, coal burning, and liquid petroleum gas (LPG) (Hui et al., 2021; Zhang, et al. 2020). Among the most abundant 20 VOC species, half were alkanes, accounting for 79% of the total alkanes measured. The C_2-C_3 alkanes mainly originate from LPG, while C_4-C_5 alkanes are considered tracers of vehicle

emissions (Fan et al., 2021). The most abundant alkene species were ethylene, propene, isoprene, and propene, representing 72% of the total alkanes. The C_2-C_3 alkenes are mainly derived from vehicle emissions and LPG (Zhang et al., 2015), whereas isoprene is a typical biogenic tracer (Maji et al., 2020). And isoprene emissions have also been reported from biomass burning e.g. from smouldering rice straw fires (Kumar et al., 2021). In the 20 most abundant VOC species, there were 6 aromatics: toluene, m p-xylene, benzene, ethylbenzene, o-xylene and p-diethylbenzene. These aromatics are the most frequently observed aromatic compounds in urban areas, originating from vehicle emissions, industrial processes, solvent use, and combustion sources (Hui et al., 2019).

3.1.2 Interannual variation of VOCs

The interannual average concentrations and contributions of VOCs during 2018–2020 are presented in Table S2. The interannual variation of the VOCs declined gradually as follows: 113.2±65.2 μg/m^3 in 2018, 90.7±52.5 μg/m^3 in 2019, and 79.1±41.7 μg/m^3 in 2020. It should be mentioned is the differences in these yearly averages are statistically significant considering the large standard deviations indicated. The trend of decrease of VOCs could be attributed to increasingly stringent policies regarding emission reduction and the influence of the COVID-19 lockdown on air quality in 2020 (Wang et al., 2021a).

The concentrations of the 20 most abundant species are listed in Table 1. Ethane and propane were the top two most abundant species in each of the three years, indicating that LPG and vehicular emissions had substantial impact on the area surrounding the sampling site (Yadav et al., 2019). The C_4-C_5 alkanes and some aromatics represent the main tracers of motor vehicle emissions (Fan et al., 2021). However, the quantities of those species were diminished in 2020, which might represent a consequence of the COVID-19 epidemic. As a tracer of coal burning, acetylene decreased gradually from 4.8±4.9 μg/m^3 in 2018 to 0.9±1 μg/m^3 in 2020.

3.1.3 Seasonal variations

As plotted in Fig. S2 and listed in Table S4, the monthly mean mixing ratios of the VOCs and compounds were investigated. The VOCs showed clear seasonal dependence with highest concentration in winter (116.5 μg/m^3) followed by spring (86.4 μg/m^3), autumn (86.1 μg/m^3), and summer (74.2 μg/m^3). Meanwhile, the seasonal variation of the group of alkanes, alkenes, alkynes, and aromatics was similar to that of the VOCs. Additionally, the monthly mean mixing ratios of the dominant and tracer species are plotted in Fig. 2. The results show that almost all VOCs had clear seasonal dependence, with highest concentrations in winter and lowest concentrations in summer. However, the mixing ratio of isoprene was highest (2.46 μg/m^3) in July and lowest (0.33 μg/m^3) in December. As a tracer of biogenic sources, isoprene showed positive correlation with T ($R^2 = 0.61$, $p < 0.01$). In addition to biogenic emissions, the seasonal variation of VOCs was mainly influenced by changes of anthropogenic sources. As a northern city of China, Zhengzhou emits substantial quantities of pollutants during the heating season in winter (Wang et al., 2019). The higher concentrations of VOCs and tracers (such as acetylene and aromatics) in winter might be derived from coal combustion (Zhang et al., 2020).

Seasonal variations in VOC concentrations are associated with several factors such as photochemical activities and meteorological conditions. In summer, VOCs are consumed under the condition of high T, strong UV radiation, and high concentration of OH radicals (Huang et al., 2019). In winter, the high level of VOCs can often be attributed to a lower boundary layer and calm weather conditions (Hui et al., 2019). Additionally, the transport of pollutants from the Beijing–Tianjin–Hebei region cannot be ignored because of the north wind that prevails in Zhengzhou in winter. The seasonal variation of VOCs in several cities was investigated and the variation trend of VOC concentrations in most studies were found similar to that observed in Zhengzhou (Liu et al., 2019; Yadav et al., 2019).

3.1.4 Diurnal variations

The diurnal variations in VOCs, trace gases (NO_2 and O_3), and meteorological parameters (T, relative humidity, WS, and UV) are shown in Fig. S3. The VOCs present negative correlation with O_3 ($R^2 = -0.82$, $p < 0.01$), whereas the diurnal variation of VOCs shows moderate consistency with the variation of NO_2 ($R^2 = 0.62$, $p < 0.01$). The high values of VOCs generally appeared in the morning with low O_3 concentrations. The peak in the morning was attributed to vehicle emission (Li et al., 2019b). Additionally, local meteorological and atmospheric processes also play important roles in the diurnal variation of VOCs in ambient air. In the early morning, the concentrations of VOCs remained high owing to stable atmospheric conditions and a shallow boundary layer height (Hui et al., 2020). The concentration of VOCs declined to the lowest value at 15:00 China Standard Time (CST), when O_3 reached a maximum level with the production and consumption rates of O_3 in equilibrium. In the afternoon, higher T and increased UV radiation intensity led to consumption of VOCs. Moreover, higher WS also accelerated the diffusion of VOCs. Subsequently, VOC concentrations gradually accumulated with the arrival of the late traffic peak, and remained at a high level throughout the night. It should be noted that VOC concentrations at night were generally higher than those during the day. Previous studies have suggested that VOCs can be oxidized by O, OH radicals, and NO_3 radicals (Atkinson and Arey, 2003). During the daytime, reactions with OH radicals and O_3 are the most important chemical reactions for VOCs, whereas the reactions with NO_3 radicals and O_3 are the main sedimentation reactions at night. Concentrations of VOCs were generally higher at night because the chemical activity of OH radicals is much higher than that of NO_3 radicals (Carter, 2010).

The mean diurnal variations of high-concentration and tracer VOCs were investigated, as shown in Fig. 3. As tracers of motor vehicle emissions (Zheng et al., 2018), i-pentane and n-pentane showed remarkable peaks at 08:00 CST that are considered to reflect vehicle emissions. Furthermore, benzene, toluene, ethylbenzene, xylene, and the C_2-C_4 alkanes also presented similar diurnal variation characteristics

that are considered to represent the substantial effect of motor vehicles. However, the mixing ratio of isoprene showed higher values in the afternoon and had a trend similar to that of T. The elevated values of isoprene in the afternoon indicated substantial emissions from biogenic sources.

3.2 Diagnostic ratios

Some VOC species are commonly used as indicators of emission sources. To characterize the seasonal differences in the contributions of the various sources, this study adopted the benzene/toluene (B/T) ratio and the i-pentane/n-pentane ratio as the preferred metrics.

The B/T ratio can be used to distinguish potential sources such as traffic emissions, coal+biomass combustion, and solvent use. The diagnostic ratios varied according to the emission sources (i.e., below 0.20 for solvent use, 0.5 for traffic sources, 1.5–2.2 for coal combustion, and 2.5 for biomass burning) (Huang et al., 2019; Li et al., 2019a). As shown in Fig. S4, the highest value of the B/T ratio was 0.55 in winter, suggesting that traffic emissions affected the ambient atmosphere. The ratios of 0.31, 0.27, and 0.31 in spring, summer, and autumn, respectively, indicate that aromatics were more likely derived from the mixed sources of solvent use and vehicle emissions during these seasons. As a transportation hub, Zhengzhou has a large number of motor vehicles (Gu et al., 2019a). Therefore, regional controls on motor vehicle use should be strengthened.

The i-pentane/n-pentane ratio was also investigated. Generally, i-pentane and n-pentane have similar reaction rates with OH radicals, and the ratio of this pair of species is indicative of different sources. The i-pentane/n-pentane ratio associated with coal combustion, vehicle emissions, and fuel evaporation is generally 0.56–0.80, ~ 2.2, and 3.8, respectively (Huang et al., 2019; Li et al., 2019a). The highest i-pentane/n-pentane ratio was found in summer (2.79), indicating strong impact from traffic sources. The ratio was 1.88 in spring and 1.96 in autumn, suggesting that most VOCs originated from the mixed sources of vehicle emissions and coal combustion.

Notably, the average ratio in winter (1.55) was lower than that in the other three seasons, indicating stronger contribution from coal burning in the heating season.

3.3 Source identification

In this study, six sources were identified using the PMF model: industrial sources, solvent use, vehicle emissions, LPG/natural gas (NG), fuel burning, and biogenic sources. The source profiles of the VOCs during the sampling period are presented in Fig. 4.

3.3.1 Factor 1: industrial sources

Factor 1 was characterized by high loadings on ethylene (60.6%), ethane (31.6%), propylene (25.8%), and propane (24.0%). Ethene and propylene are the first and second most abundant industrially produced organic compounds worldwide, respectively (Eckert et al., 2014). Additionally, this factor was also dominated by aromatics such as styrene (76.0%), toluene (34.3%), and ethylbenzene (28.1%), which are typical tracers of industrial sources. Meanwhile, this source had correlation with gas tracers of NO_2, SO_2, and CO (R^2 = 0.47, 0.36, and 0.49, respectively). CO and NO2 are mainly gases from combustions sources strongly influenced by urban activities such as traffic and domestic heating. Instead, SO_2 is generally mainly due to industrial sources or combustion of heavy oils and coals. Therefore, source 1 was assigned to industrial sources.

The CPF plots indicated the dominant source directions as northeast and southeast, which correspond to industrial estates (as shown in Fig. 5). Moreover, the highest VOC concentration from industrial sources was observed at 10:00 CST, probably attributable to increased industrial activities during daytime.

3.3.2 Factor 2: solvent use

Factor 2 was characterized by high levels of n-hexane (60.4%), n-octane (26.3%), methyl cyclohexane (20.4%), o-xylene (79.6%), m/p-xylene (61.7%), p-

diethylbenzene (84.0%), o-xylene (79.0%), m-ethyl toluene (57.8%), o-ethyl toluene (29.2%), ethylbenzene (51.1%), and toluene (20.8%). These compounds are major components emitted through the use of various solvents or industrial processes (Zhou et al. 2019, Wang et al. 2021). However, there were almost no tracers of ethane, ethene, acetylene, and benzene related to combustion sources, and this source appeared to exhibit poor correlation with gas tracers ($R^2 < 0.10$). Therefore, source 2 was identified as solvent use.

The CPF plots of this factor suggested southeast was the dominant source direction, possibly reflecting the presence of the large manufacturers of automobiles in the southeastern urban area.

3.3.3 Factor 3: vehicle emissions

Factor 3 was identified by high percentages of C2-C6 alkanes (i.e., ethane (37.8%), propane (46.9%), iso-butane (40.9%), n-butane (38.5%), n-pentane (26.0%), and i-pentane (31.6%)), C2-C4 alkanes (i.e., ethylene (31.4%), propylene (38.4%), and 1-butene (67.4%)), and C6-C8 aromatics (i.e., benzene (21.4%), toluene (30.7%), and m/p-xylene (25.6%)). These components are considered typical products of incomplete combustion processes (Baudic et al., 2016; Gaimoz et al., 2011; Liu et al., 2008a; Song et al., 2018). It is reported that i-pentane usually originates from gasoline evaporation (Mo et al., 2017), and that 2-methylpentane and 3-methylpentane are tracers of the emissions of gasoline-powered vehicles (Tsai et al., 2003; Liu et al., 2008; Song et al., 2018). The T/B ratio was 2.0 in this profile, which further confirms the effect of vehicular emissions (Yao et al., 2021). Moreover, the source correlated significantly with CO and NO_2 ($p < 0.01$), but not with SO_2 ($p > 0.05$); therefore, source 3 was identified as vehicle emissions.

Factor 3 showed larger CPF values when the wind came from the north, possibly because the site is adjacent to Jinshui Road, which is the main road in Zhengzhou. The diurnal pattern of the traffic source was characterized by two peaks: one in the morning and the other in the evening, consistent with the relative strength of local

traffic flow.

3.3.4 Factor 4: LPG/NG

Factor 4 was dominated by strong presence of ethane (16.3%), propane (14.6%), iso-butane (38.9%), n-butane (44.4%), n-pentane (60.3%), and i-pentane (66.2%), which can also be released via fuel evaporation (gasoline and LPG/NG) (Zhang et al., 2019). Pentanes are the most abundant VOC species associated with gasoline evaporation (Liu et al., 2008; Zhang et al., 2013; Shen et al., 2018), and butanes are reported as tracers of LPG (McCarthy et al., 2013). In particular, the aromatics of this source were very low. Similar to factor 3, the source did not correlate with SO_2 ($p > 0.05$), but had positive correlation with both CO and NO_2 ($p < 0.01$); therefore, this source was considered as LPG/NG.

The dependence of factor 4 on WD was not as significant as for other sources. It is related to compact residential areas with greater human activity. There are residential areas around the monitoring site, and LPG/NG leakage might have occurred in the process of daily life.

3.3.5 Factor 5: fuel burning

Factor 5 was distinguished by substantial amounts of acetylene (72%), which is a marker of combustion sources (Hui et al., 2021). Additionally, the source was also characterized by considerable amounts of benzene and C_2-C_3 hydrocarbons, which are representative species of incomplete combustion processes (Zheng et al., 2021). Meanwhile, the independent tracers (i.e., NO_2, SO_2, and CO) exhibited correlation with this factor ($R^2 > 0.3$, $p < 0.01$); therefore, source 5 was considered to be fuel burning.

Factor 5 displayed high CPF values when the wind was from east. This is possibly related to the heating companies located within 1.0 km to the east of the site. The diurnal variation of this factor was characterized by apparent increase at night, which could be related to the accumulation of pollutants associated with nighttime

heating.

3.3.6 Factor 6: biogenic sources

Factor 6 exhibited a significantly high composition of isoprene, which is mainly produced by vegetation through photosynthesis (Song et al., 2019a). Accordingly, source 6 was labeled as biogenic sources.

The CPF plots indicated that this factor mainly originated from the west with conditional probability values of approximately 0.44. It is mainly affected by Zijinshan Park, which is located ~1 km to the west of the monitoring site. Additionally, the diurnal pattern of the biogenic sources showed obvious T dependence, with the highest concentration at midday that could be associated with photosynthetic activity.

3.3.7 Comparison between the composite source profiles and the PMF factors

As shown in Fig. S5, the source profiles derived from the PMF analysis were compared with their sources attributed from the source profiles. The data of the source profiles were derived from a local tunnel experiment and a review of the most recent literature. The source profiles for solvent use correlated most strongly between the two methods (R = 0.84). A study by Jin et al. (2022) identified that low-carbon alkanes (e.g., ethane, propane, and isopentane), alkenes (e.g., ethylene, propene, and 1-butene), and aromatics (e.g., benzene, toluene, and m/p-xylene) were the main groups in the tunnel study, and that vehicle emissions agreed well between this factor and the source profiles (R = 0.59). Different profiles of combustion sources were investigated, and the correlation between the results of NG combustion and the PMF factor was strongest (R = 0.57). The above results are to be expected because Zhengzhou has gradually phased out coal-fired boilers and replaced them with gas boilers in recent years. As for industrial sources, the correlation between the two methods was 0.43. The C_2-C_3 hydrocarbons accounted for a high proportion in factor 1, whereas the content of aromatics was lower. Industrial production of nonmetallic

462 mineral products in Zhengzhou is reasonably well developed, which leads to large
463 emissions of ethane and propane. The main contributing source of aromatic
464 hydrocarbons is rubber and plastics. However, the scale of the enterprises involved in
465 their production is far lower than that in the Pearl River Delta; consequently, the
466 emission of aromatic hydrocarbons is lower in Zhengzhou.

467 **3.4 VOC source contributions**

468 **3.4.1 Interannual variation**

469 The concentration contributions of each VOC source during 2018–2020 are
470 shown in Fig. 6. In 2018, vehicular emissions were the largest contributor to VOC
471 mixing ratios (32%), followed by industrial sources (21%), solvent use (19%), and
472 LPG/NG (15%). The contribution of fuel burning and biogenic sources accounted for
473 9% and 4% of the total VOC concentration, respectively. As for 2019, vehicle
474 emissions made the largest contribution (38%) to atmospheric VOCs. The second
475 most significant source was industrial sources, accounting for 18% of the total. The
476 contribution of solvent use, LPG/NG, fuel burning, and biogenic sources to
477 atmospheric VOCs was 17%, 15%, 11%, and 2%, respectively, in 2019. Vehicular
478 emissions, LPG/NG, industrial sources, solvent use, fuel burning, and biogenic
479 sources accounted for 39%, 18%, 17%, 15%, 9%, and 3%, respectively, in 2020
480 In summary, vehicle emissions and industrial sources made the largest
481 contributions in all three years. Moreover, the proportions of the contributions of
482 vehicle emissions and LPG/NG have increased with each passing year. As a
483 transportation hub city, the number of motor vehicles in Zhengzhou has maintained a
484 rate of growth of 0.4 million annually during the past five years, and the total number
485 of vehicles exceeded 4.5 million in 2020 (Gu et al., 2019a). Thus, vehicle emissions
486 represent an important source of ambient VOCs in Zhengzhou. Both LPG and NG are
487 used widely in residential life, industrial production, and motor vehicles. In terms of
488 the actual situation of the monitoring site, residential emissions might represent the
489 main source of LPG/NG. With adjustment of the energy structure, most industrial

enterprises and taxis in Zhengzhou now use NG as energy or fuel. It should be noted that the proportion of the contributions from industrial and solvent sources has presented an annual downward trend. In recent years, Zhengzhou has implemented special actions designed to reduce VOC emissions, focusing on the control of industrial and scattered small-scale pollution enterprises. According to the results obtained using the PMF model, it is speculated that the effect of such policy control has been remarkable.

3.4.2 Seasonal variation

Owing to different meteorological conditions and emission strengths, the source contributions vary seasonally. As shown in Fig. 7, the seasonal variation of biogenic emissions was substantial, with the highest contribution in summer (7%) and the lowest contribution in winter (<1%). This might reflect both T and UV intensity. Conversely, the contributions from fuel burning were larger in winter and lower in summer. Fuel burning accounted for a larger proportion of emissions in winter (17%) than in summer (3%). Meanwhile, industrial emissions contributed a high percentage of VOCs in spring (22%), whereas the contributions in the other three seasons were comparable. Additionally, motor vehicle emissions showed no obvious seasonal characteristics, and the contribution to atmospheric VOCs in each of the four seasons exceeded 30% of the total, indicating that motor vehicles have considerable impact on the air quality of Zhengzhou.

3.4.3 Comparison with other studies

3.4.3.1 Comparison with emission inventory (EI) studies

This study compared the annual average relative contributions of different sources with results from published emission inventory (EI) studies. In the anthropogenic VOC emission inventories established by Lu et al. (2020), VOC sources were classified into eight categories: stationary combustion, on-road mobile sources, non-road mobile sources, industrial processes, solvent use sources, fuel oil

storage and transportation, biomass burning, and others. Vehicle emissions represented the most abundant source of anthropogenic VOCs in both the EI and the PMF analysis, accounting for 29.7% and 36.3% of the total, respectively. The differences observed between the EI and PMF results were primarily because most of the vehicles considered were in urban areas. The contributions of industrial sources and of solvent use sources represented the second and third largest, respectively, in both the EI and the PMF results. However, the overall contribution of those two sources obtained from the PMF results was lower than that derived from the EI analysis. The relative contribution of combustion sources resolved from the PMF analysis was higher than that obtained from the EI results, accounting for 9.5% and 4.3%, respectively. Such large differences occurred primarily because of uncertainties in the activity data obtained from statistical information. Residential energy consumption and emissions were poorly recorded in comparison with other sources (Chen et al., 2016; Tao et al., 2018), leading to higher uncertainties in the related estimations of such emissions. Thus, it is necessary to estimate the emissions of residential fossil fuel combustion through scientific approaches.

3.4.3.2 Comparison with other PMF studies

The source contributions determined in this research were also compared with the results from other studies. It can be seen from Table 2 that the source apportionment of VOCs in this study was broadly within the values reported for other Chinese cities (Huang et al., 2019; Hui et al., 2018; Li et al., 2020c; Mo et al., 2017; Yan et al., 2017). It was found that traffic emissions represent the main source of VOCs in Zhengzhou and the other five cities, indicating that vehicle emissions have considerable impact on the concentration of VOCs in the urban atmosphere. It should be noted that the contribution of each source determined in this study was very similar to that reported for Wuhan (Hui et al., 2018). Given that Zhengzhou and Wuhan are both important transportation hub cities in central China, this result is in line with expectation.

3.5 AOC

The AOC during the sampling periods was quantified, as shown in Fig. 8. The calculated averaged value of total AOC was 7.4×10^7 molecules cm^{-3} s^{-1}, comparable with values reported for a suburban site between Beijing and Tianjin (Yang et al., 2020b), but substantially higher than observed in Shanghai (Zhu et al., 2020), Hong Kong (Xue et al., 2016), Chile (Elshorbany et al., 2009), and Berlin (Geyer et al., 2001). Among the AOC categories, OH exhibited the highest average concentration (7.0×10^7 molecules cm^{-3} s^{-1}), accounting for 95% of the total AOC, followed by O_3 (3.4×10^6 molecules cm^{-3} s^{-1}) and NO_3 (1.1×10^5 molecules cm^{-3} s^{-1}), which contributed 4% of the total AOC. Thus, OH is the main contributor of atmospheric oxidation in Zhengzhou, similar to the results reported for other regions by other studies (Yang et al., 2021; Zhu et al., 2020).

During 2018–2020, the total AOC presented a decreasing trend annually (as shown in Fig. 8), with mean values of 8.0, 6.4, and 6.2×10^7 molecules cm^{-3} s^{-1}, respectively. As expected, OH was the predominant oxidant in each of the three years, accounting for 95%, 95%, and 97% of the total AOC, respectively. The primary pollutants (e.g., CO, CH_4, and VOCs) decreased significantly in 2020 owing to large reductions in economic activity and the associated emissions during the COVID-19 lockdown. However, the average OH concentration was highest in 2020 (4.8×10^7 molecules cm^{-3}), far higher than that in either of the two previous years. Thus, the level of atmospheric oxidation needs additional attention. It should be noted that oxidation of the atmosphere did not decrease or even increase significantly during the epidemic, which has been reported by many previous studies (Wang et al., 2021b).

As shown in Fig. S7, the mean AOC values showed pronounced seasonal variation. The highest total AOC value was detected in summer (7.5×10^7 molecules cm^{-3} s^{-1}), followed by winter (6.4×10^7 molecules cm^{-3} s^{-1}), spring (5.8×10^7 molecules cm^{-3} s^{-1}), and autumn (5.7×10^7 molecules cm^{-3} s^{-1}). The concentration of OH in summer was significantly higher than that in the other seasons, which can be ascribed to the relatively favorable meteorological conditions. Meanwhile, high

concentrations of isoprene were observed in summer, and its high reaction rate coefficients with oxidants (e.g., OH, NO_3, and O_3) revealed a highly oxidative environment during the summer campaign in Zhengzhou. This seasonal pattern of the AOC is similar to that found in other studies conducted at the national level, and in urban and suburban environments (Yang et al., 2021; Li et al., 2020a).

3.6 Atmospheric environmental implications

3.6.1 OH reactivity of measured species

The calculated OH reactivity was categorized into SO_2, NO_2, NO, O_3, CO, and VOCs, as shown in Fig. 9. During the sampling period, the average value of total OH reactivity was 45.3 s^{-1}. Generally, the OH reactivity assessed in this study was much higher than that determined in Shanghai (Tan et al., 2019; Zhu et al., 2020), Chongqing (Tan et al., 2019), and New York (Ren et al., 2006), but comparable with or lower than that reported in Xianghe (Yang et al.,2020a) and Backgarden (Lou et al., 2010). In Zhengzhou, NO_2 made the largest contribution to total OH reactivity (54%), followed by VOCs (17%), NO (16%), CO (11%), SO_2 (3%), and O_3 (1%). Similar results were reported by previous studies conducted in other regions (Yang et al., 2021). It should be noted that this study calculated only the OH reactivity of the measured species, i.e., the impact of unmeasured species, such as secondary products (oxygenated VOCs and nitrates produced by photochemical reactions) and monoterpenes, were not considered. Previous studies have shown that both undetected primary emissions and unmeasured secondary products could contribute to missing reactivity (Yang et al., 2016). Therefore, the value of OH reactivity determined in this study was underestimated to a certain extent.

OVOCs play an important role to influence the AOC via OH-initiated degradation. A previous review suggested that missing OH reactivity has often been observed, and the difference compared the measured and calculated was attributed to a lack of measurement data for OVOCs (Yang et al., 2016). Steiner et al. (2008) found that OVOCs accounted for 30–50% of the modelled urban VOC reactivity by using

the regional Community Multiscale Air Quality model (CMAQ). In another urban study, OVOCs were found to contribute between 11–24% during summertime in Houston (Mao et al., 2010b). In the CareBeijing-2006 and PRIDE-PRD campaigns, Lou et al., (2010) and lu et al., (2013) reported the significant contributions of OVOCs to OH reactivity based on model simulations. Since OVOCs were not simultaneously measured in four Chinese megacities, the OVOC contributions were simulated with a box model. And OVOCs explained between 20% and 23% to the total OH reactivity (Tan et al., 2019). In summary, OVOCs behaved as a major contributor to the total OH reactivity.

Table S5 shown the OH reactivity towards the total VOCs and the comparison with other studies. The OH reactivity of the total VOCs was 6.7 s^{-1}, i.e., much lower than that reported for Heshan (13.6 s^{-1}) (Yang et al., 2017) and Beijing (8.3 s^{-1}) (Yang et al., 2021), but close to that found in Guangzhou (6.4 s^{-1}) and Chongqing (6.8 s^{-1}) (Tan et al., 2019) and higher than that determined in Shanghai (3.2 s^{-1}) (Tan et al., 2019). The detailed contributions of each VOC group to total OH reactivity are presented in Tables S6 and S7. The contribution of alkenes to OH reactivity was predominant, accounting for 5.2 s^{-1} of the total OH reactivity of VOCs. During the sampling period, isoprene made the largest contribution to the OH reactivity of the total VOCs, followed by ethene, m/p-xylene, propene, styrene, cis-2-butene, trans-2-butene, toluene, i-pentane, and trans-2-pentene, which collectively accounted for 70% of the OH reactivity of the total VOCs.

As shown in Fig. 9, OH reactivity showed substantial interannual and seasonal variations. The statistical results exhibit a decreasing trend of OH reactivity during 2018–2020 in Zhengzhou with mean values of 50.2, 46.9, and 36.9 s^{-1}, respectively. This trend might reflect the implementation of emission reduction measures such as traffic-related measures and the “Coal to Gas” project. The OH reactivity in 2020 was 21% lower than that in the previous year, which is closely related to the emission reduction associated with the COVID-19 epidemic. Seasonally, the mean value of OH reactivity decreased in the following order: winter (74.5 s^{-1}) > autumn (48.6 s^{-1}) > spring (43.1 s^{-1}) > summer (31.8 s^{-1}). The notable differences might be attributable to

higher loadings of reactive trace gases, especially NOx and CO. As a northern city, coal combustion in Zhengzhou during the heating season produces higher concentrations of NOx and CO, leading to higher OH reactivity. Therefore, we should continually strengthen policies to control trace gases, especially in autumn and winter. The OH reactivity of the total VOCs was similar with the higher value in winter (7.3 s^{-1}) and the lower value in autumn (5.3 s^{-1}). However, the concentrations of the key species were markedly different among the four seasons. Ethylene and propylene had highest OH reactivity in winter, which is speculated to be related to the emission of combustion sources. Additionally, isoprene made the largest contribution to the total OH reactivity in both summer and spring, reflecting the substantial effect of biogenic sources. Overall, the research on specific OH reactivity clearly elucidated the seasonal and annual variations of the major reactants. Therefore, control strategies based on OH reactivity should focus on the key species.

3.6.2 Effect of VOCs on O_3 formation

Because VOCs are important precursors of O_3 formation in the ground-level atmosphere, it is necessary to adequately estimate the contribution of each VOC species to O_3 formation. The concentration contributions of the four VOCs categories expressed on different scales from 2018–2020 are shown in Fig. S8. The result suggests that aromatics made the largest contribution to the MIR concentration, accounting for a combined ratio of 81%. Meanwhile, alkenes were the largest contributors to the PE concentration (87%). Although the concentrations of aromatics and alkenes are relatively low, these two VOC groups play an important role in O_3 formation, which is a result supported by many previous studies (Hui et al., 2021; Li et al., 2020b). It should be noted that the effect of VOCs on O3 formation were calculated from the sum of measured species, and does not involve species that were not measured, such as OVOCs. Therefore, we provided a lower limit of the effect of VOCs on O_3 formation in this study.

Among the top 10 reactive species contributing to the PE and MIR weighted

concentrations (as shown in Fig. 10), 8 compounds were the same, differing only in their rank order.The top 10 VOCs obtained from the PE and MIR methods represent 67% and 74% of VOCs, respectively. Considering kinetic activity, isoprene ranked first (8.8 ppbC) with the PE method, accounting for approximately 20% of the total PE concentration, and m,p-xylene, styrene, ethene, and toluene ranked second to fifth, explaining 16%, 10%, 7%, and 5% of the total OFP, respectively. In comparison, ethene, m/p-xylene, toluene, propane, and isoprene had the highest MIR concentrations, which accounted for approximately 23%, 21%, 12%, 7%, and 7%, respectively. The results of this study highlight the contributions of isoprene, ethene, m/p-xylene, and toluene to O_3 formation, and these species are derived primarily from vehicle emissions and industrial coatings (Xiong and Du, 2020).

On the basis of the results of source apportionment, the source contributions to OFP and PE were calculated (shown in Fig. S9). Vehicle emissions made the greatest contribution to O_3 formation (OFP: 23%; PE: 29%), followed by solvent use (OFP: 25%; PE: 24%). However, the contribution of biogenic emissions accounting for 22% of the total PE cannot be ignored. Because of the discrepancy between the MIR weighted and PE weighted concentrations, the contribution of this source to OFP was relatively low, accounting for only 6%. The PE concentration method considers only the kinetic reactivity of VOC species and ignores mechanism reactivity, whereas the MIR method considers the impact of the VOC/NOx ratio on O_3 formation.

4. Conclusions

In this study, hourly observational data of 57 VOC species were collected during 2018–2020 at an urban site in Zhengzhou (China). The results showed that the average total VOC mixing ratio was 94.3±53.1 μg/m3 (38.2±15.6 ppbv), and that the VOC concentrations were dominated by alkanes in each of the three years. During the sampling period, the interannual variation of VOCs gradually reduced as follows: 113.2±65.2 μg/m3 in 2018, 90.7±52.5 μg/m3 in 2019, and 79.1±41.7 μg/m3 in 2020. The VOCs showed clear seasonal dependence with the highest value in winter (116.5

688 μg/m^3) and lowest value in summer (74.2 μg/m^3). The PMF method was used to
689 identify six sources: vehicle emissions (36%), solvent use (17%), LPG/NG (16%),
690 industrial sources (18%), fuel burning (10%), and biogenic sources (3%). The
691 proportion of both vehicle emissions and LPG/NG has increased with each passing
692 year. However, the proportion of industrial and solvent sources presented a decreasing
693 trend. In addition to substantial interannual variation, the VOC sources also showed
694 marked seasonal differences. The contribution of vehicle emissions to the atmosphere
695 in each of the four seasons was >30%. Atmospheric VOCs are affected substantially
696 by fuel burning (17%) in winter; however, the influence of biogenic sources cannot be
697 ignored (7%) in summer.

698 This study also focused on the atmospheric environmental implications of VOCs,
699 including the AOC, OH reactivity, and OFP. During the sampling periods, the
700 campaign-averaged value of the total AOC was 7.4×10^7 molecules cm^{-3} s^{-1}, and OH
701 exhibited the highest average concentration, accounting for 95% of the total AOC.
702 The average value of the total OH reactivity was 45.3 s^{-1}, and NO_2 made the largest
703 contribution to the total OH reactivity (54%), followed in descending order by VOCs
704 (17%), NO (16%), CO (11%), SO_2 (3%), and O_3 (1%). Investigation of the effects of
705 VOCs on O_3 formation revealed that despite the relatively low concentrations of
706 aromatics and alkenes, they played important roles in O_3 formation. Ethene,
707 m/p-xylene, and toluene contributed substantially to O_3 formation in Zhengzhou. The
708 source apportionment results indicate that vehicle emissions and solvent use remain
709 the key sources of the VOCs that contribute to O_3 formation.

710 Overall, investigation of the concentrations, source apportionment, and
711 atmospheric environmental implications clearly elucidated the differences in the
712 major reactants observed in different seasons and years. Therefore, control strategies
713 should consider seasonal and interannual variations when focusing on the key species
714 and sources. The results of this study could support local governments in developing
715 strategies to control VOCs during O_3 pollution events.

716

717

Data availability

The data set is available to the community and can be accessed by request from Ruiqin Zhang (rqzhang@zzu.edu.cn).

Author contribution

YSJ and ZRQ planned and organized the study, and were deeply involved in writing the manuscript. WSB, XRX and ZD performed the atmospheric measurements and data analysis and wrote the manuscript. ZM and WLL assisted heavily with the atmospheric measurements and data analysis. SFC and LX and LX conducted the model development and data analysis.

Other coauthors provided useful insights in data analysis and contributed to the writing of the manuscript.

We thank James Buxton, MSc, from Liwen Bianji (Edanz) (www.liwenbianji.cn/), for editing the English text of a draft of this manuscript.

Acknowledgments

This work was supported by the Study of Collaborative Control of $PM_{2.5}$ and O_3 Pollution in Zhengzhou City (No. 20200321A) and National Key Research and Development Program of China (No. 2017YFC0212403).

References

Atkinson, R., Arey, J., 2003. Atmospheric degradation of volatile organic compounds. Chem. Rev. 103, 4605-4638.

Atkinson, R., Baulch, D., Cox, R., Crowley, J., Hampson, R., Hynes, R., Jenkin, M., Rossi, M., Troe, J., 2004. Evaluated kinetic and photochemical data for atmospheric chemistry: volume I - gas phase reactions of Ox, HOx, NOx and SOx species. Atmos. Chem. Phys. 4, 1461-1738.

Baudic, A., Gros, V., Sauvage, S., Locoge, N., Sanchez, O., Sarda-Estève, R., Kalogridis, C., Petit, J.E., Bonnaire, N., Baisnée, D., Favez, O., 2016. Seasonal variability and source apportionment of volatile organic compounds (VOCs) in the Paris megacity (France). Atmos. Chem. Phys. 16, 11961–11989.

Carter, W., 1994. Development of ozone reactivity scales for volatile organic compounds. J. Air Waste Manag. Assoc. 44, 881-899.

Carter, W., 2010. Development of the SAPRC-07 chemical mechanism. Atmos. Environ. 44, 5324-5335.

Elshorbany, Y., Kurtenbach, R., Wiesen, P., Lissi, E., Rubio, M., Villena, G., Gramsch, E., Rickard, A., Pilling, M., Kleffmann, J., 2009. Oxidation capacity of the city air of Santiago, Chile. Atmos. Chem. Phys. 9, 2257-2273.

Fan, M., Zhang, Y., Lin, Y., Li, L., Xie, F., Hu, J., Mozaffar, A., Cao, F., 2021. Source apportionments of atmospheric volatile organic compounds in Nanjing, China during high ozone pollution season. Chemosphere. 263, 128025.

Fu, S., Guo, M., Luo, J., Han, D., Chen, X., Jia, H., Jin, X., Liao, H., Wang, X., Fan, L., Cheng, J., 2020. Improving VOCs control strategies based on source characteristics and chemical reactivity in a typical coastal city of South China through measurement and emission inventory. Sci. Total Environ. 744, 140825.

Gao, J., Zhang, J., Li, H., Li, L., Xu, L., Zhang, Y., Wang, Z., Wang, X., Zhang, W., Chen, Y., Cheng, X., Zhang, H., Peng, L., Chai, F., Wei, Y., 2018. Comparative study of volatile organic compounds in ambient air using observed mixing ratios

767 and initial mixing ratios taking chemical loss into account - A case study in a
768 typical urban area in Beijing. Sci. Total Environ. 628-629, 791-804.

769 Garzn, J., Huertas, J., Magaa, M., Huertas, M., Crdenas, B., Watanabe, T., Maeda, T.,
770 Wakamatsu, S., Blanco, S., 2015. Volatile organic compounds in the atmosphere
771 of Mexico city. Atmos. Environ. 119, 415-429.

772 Geyer, A., Alicke, B., Konrad, S., Schmitz, T., Stutz, J., Platt, U., 2001. Chemistry and
773 oxidation capacity of the nitrate radical in the continental boundary layer near
774 Berlin. J. Geophys. Res.-Atmos. 106, 8013-8025.

775 Gu, X., Yin, S., Lu, X., Zhang, H., Wang, L., Bai, L., Wang, C., Zhang, R., Yuan, M.,
776 2019a. Recent development of a refined multiple air pollutant emission inventory
777 of vehicles in the central plains of China. J. Environ. Sci (in China). 84, 80-96.

778 Gu, Y., Li, Q., Wei, D., Gao, L., Tan, L., Su, G., Liu, G., Liu, W., Li, C., Wang, Q.,
779 2019b. Emission characteristics of 99 NMVOCs in different seasonal days and
780 the relationship with air quality parameters in Beijing, China. Ecotoxicol.
781 Environ. Saf. 169, 797-806.

782 Gu, Y., Liu, B., Li, Y., Zhang, Y., Bi, X., Wu, J., Song, C., Dai, Q., Han, Y., Ren, G.,
783 Feng, Y., 2020. Multi-scale volatile organic compound (VOC) source
784 apportionment in Tianjin, China, using a receptor model coupled with 1-hr
785 resolution data. Environ. Pollut. 265, 115023.

786 Guo, H., Cheng, H., Ling, Z., Louie, P., Ayoko, G., 2011. Which emission sources are
787 responsible for the volatile organic compounds in the atmosphere of Pearl River
788 Delta. J. Hazard. Mater. 188, 116-124.

789 Hsu, C., Chiang, H., Shie, R., Ku, C., Lin, T., Chen, M., Chen, N., Chen, Y., 2018.
790 Ambient VOCs in residential areas near a large-scale petrochemical complex:
791 Spatiotemporal variation, source apportionment and health risk. Environ. Pollut.
792 240, 95-104.

793 Huang, X., 2020. Evaluating the effectiveness of multiple emission control measures
794 on reducing volatile organic compounds in ambient air based on observational
795 data: A case study during the 2010 Guangzhou Asian Games. Sci. Total Environ.

723, 138171.

Huang, Y., Hsieh, C., 2019. Ambient volatile organic compound presence in the highly urbanized city: source apportionment and emission position. Atmos. Environ. 206, 45-59.

Hui, L., Liu, X., Tan, Q., Feng, M., An, J., Qu, Y., Zhang, Y., Jiang, M., 2018. Characteristics, source apportionment and contribution of VOCs to ozone formation in Wuhan, Central China. Atmos. Environ. 192, 55-71.

Hui, L., Liu, X., Tan, Q., Feng, M., An, J., Qu, Y., Zhang, Y., Cheng, N., 2019. VOC characteristics, sources and contributions to SOA formation during haze events in Wuhan, Central China. Sci. Total Environ. 650, 2624-2639.

Hui, L., Liu, X., Tan, Q., Feng, M., An, J., Qu, Y., Zhang, Y., Deng, Y., Zhai, R., Wang,Z., 2020. VOC characteristics, chemical reactivity and sources in urban Wuhan, central China. Atmos. Environ. 224,117340.

Hui, L., Ma, T., Gao, Z., Gao, J., Wang, Z., Xue, L., Liu, H., Liu, J., 2021. Characteristics and sources of volatile organic compounds during high ozone episodes: A case study at a site in the eastern Guanzhong Plain, China. Chemosphere. 265,129072.

Jiang, N., Duan, S., Yu, X., Zhang, R., Wang, K., 2018. Comparative major components and health risks of toxic elements and polycyclic aromatic hydrocarbons of $PM_{2.5}$ in winter and summer in Zhengzhou: Based on three-year data. Atmos. Res. 213, 173-184.

Li, B., Ho, S., Gong, S., Ni, J., Li, H., Han, L., Yang, Y., Qi, Y., Zhao, D., 2019a. Characterization of VOCs and their related atmospheric processes in a central Chinese city during severe ozone pollution periods. Atmos. Chem. Phys. 19, 617-638.

Li, K., Li, J., Tong, S., Wang, W., Huang, R.-J., Ge, M., 2019b. Characteristics of wintertime VOCs in suburban and urban Beijing: concentrations, emission ratios, and festival effects. Atmos. Chem. Phys. 19, 8021-8036.

824 Li, Q., Badia, A., Wang, T., Sarwar, G., Fu, X., Zhang, L., Zhang, Q., Fung, J., Cuevas,
825 C., Wang, S., Zhou, B., Saiz-Lopez, A., 2020a. Potential effect of halogens on
826 atmospheric oxidation and air quality in China. J. Geophys. Res-atmos. 125,
827 e2019JD032058.

828 Li, Y., Yin, S., Yu, S., Yuan, M., Dong, Z., Zhang, D., Yang, L., Zhang, R., 2020b.
829 Characteristics, source apportionment and health risks of ambient VOCs during
830 high ozone period at an urban site in central plain, China. Chemosphere. 25,
831 126283.

832 Li, Q., Su, G., Li, C., Liu, P., Zhao, X., Zhang, C., Sun, X., Mu, Y., Wu, M., Wang, Q.,
833 Sun, B., 2020c. An investigation into the role of VOCs in SOA and ozone
834 production in Beijing, China. Sci. Total. Environ. 720, 137536.

835 Liebmann, J., Muller, J., Kubistin, D., Claude, A., Holla, R., Plass-Dülmer, C.,
836 Lelieveld, J., Crowley, J., 2018. Direct measurements of NO_3 reactivity in and
837 above the boundary layer of a mountaintop site: identification of reactive trace
838 gases and comparison with OH reactivity. Atmos. Chem. Phys. 18, 12045-12059.

839 Liu, B., Liang, D., Yang, J., Dai, Q., Bi, X., Feng, Y., Yuan, J., Xiao, Z., Zhang, Y., Xu,
840 H., 2016. Characterization and source apportionment of volatile organic
841 compounds based on 1-year of observational data in Tianjin, China. Environ.
842 Pollut. 218, 757-769.

843 Liu, Y., Song, M., Liu, X., Zhang, Y., Hui, L., Kong, L., Zhang, Y., Zhang, C., Qu, Y.,
844 An, J., Ma, D., Tan, Q., Feng, M., 2019a. Characterization and sources of volatile
845 organic compounds (VOCs) and their related changes during ozone pollution
846 days in 2016 in Beijing, China. Environ. Pollut. 257, 113599.

847 Liu, Y., Wang, H., Jing, S., Gao, Y., Peng, Y., Lou, S., Cheng, T., Tao, S., Li, L., Li, Y.,
848 Huang, D., Wang, Q., An, J., 2019b. Characteristics and sources of volatile
849 organic compounds (VOCs) in Shanghai during summer: Implications of
850 regional transport. Atmos. Environ. 215, 116902.

851 Lou, S., Holland, F., Rohrer, F., Lu, K., Bohn, B., Brauers, T., Chang, C., Fuchs, H.,

852 Häseler, R., Kita, K., Kondo, Y., Li, X., Shao, M., Zeng, L., Wahner, A., Zhang,
853 Y., Wang, W., and Hofzumahaus, A., 2010. Atmospheric OH reactivities in the
854 Pearl River Delta – China in summer 2006: measurement and model results,
855 Atmos. Chem. Phys. 10, 11243-11260.
856 Maji, S., Beig, G., Yadav, R., 2020. Winter VOCs and OVOCs measured with
857 PTR-MS at an urban site of India: Role of emissions, meteorology and
858 photochemical sources. Environ. Pollut. 258,113651.
859 Mao, J., Ren, X., Chen, S., Brune, W., Chen, Z., Martinez, M., Harder, H., Lefer, B.,
860 Rappengluck, B., Flynn, J., Leuchner, M., 2010. Atmospheric oxidation capacity
861 in the summer of Houston 2006: comparison with summer measurements in
862 other metropolitan studies. Atmos. Environ. 44, 4107-4115.
863 Mo, Z., Shao, M., Lu, S., Niu, H., Zhou, M., Sun, J., 2017. Characterization of
864 non-methane hydrocarbons and their sources in an industrialized coastal city,
865 Yangtze River Delta, China. Sci. Total. Environ. 593-594, 641-653.
866 Norris, G., Duvall, R., Brown, S., Bai, S., 2014. EPA Positive Matrix Factorization
867 (PMF) 5.0 Fundamentals and User Guide, U.S. Environmental Protection
868 Agency National Exposure Research Laboratory Research Triangle Park, NC.
869 Prinn, R., 2003. The cleansing capacity of the atmosphere. Annu. Rev. Environ.
870 Resour. 28, 29-57.
871 Ren, Y., Ma, S., Wang, W., Yu, S., Li, Y., Zhang, R., Yin, S., 2020. Ambient VOCs
872 characteristics, ozone formation potential, and source apportionment of air
873 pollution in spring in Zhengzhou. Environ. Sci (in Chinese). 41, 2577-2585.
874 Ren, X., Brune, W., Mao, J., Mitchell, M., Lesher, R., Simpas, J., Metcalf, A., Schwab,
875 J., Cai, C., Li, Y., 2006. Behavior of OH and HO_2 in the winter atmosphere in
876 New York City. Atmos. Environ. 40, 252-263.
877 Sadeghi, B., Pouyaei, A., Choi, Y., Rappenglueck, B., 2022. Influence of seasonal
878 variability on source characteristics of VOCs at Houston industrial area. Atmos.
879 Environ. 277, 1190.

880 Schneidemesser, E., Monks, P., Plass-Duelmer, C., 2010. Global comparison of VOC
881 and CO observations in urban areas. Atmos. Environ. 44, 5053–5064.

882 Song, M., Tan, Q., Feng, M., Qu, Y., Liu, X., An, J., Zhang, Y., 2018. Source
883 apportionment and secondary transformation of atmospheric nonmethane
884 hydrocarbons in Chengdu, southwest China. J. Geophys. Res.Atmos. 123,
885 9741-9763.

886 Song, C., Liu, B., Dai, Q., Li, H., Mao, H., 2019a. Temperature dependence and
887 source apportionment of volatile organic compounds (VOCs) at an urban site on
888 the north China plain. Atmos. Environ. 207, 167-181.

889 Song, M., Liu, X., Zhang, Y., Shao, M., Lu, K., Tan, Q., Feng, M., Qu, Y., 2019b.
890 Sources and abatement mechanisms of VOCs in southern China. Atmos. Environ.
891 201, 28-40.

892 Song, S., Shon, Z., Kang, Y., Kim, K., Han, S., Kang, M., Bang, J., Oh, I., 2019c.
893 Source apportionment of VOCs and their impact on air quality and health in the
894 megacity of Seoul. Environ. Pollut. 247, 763-774.

895 Tan, Z., Lu, K., Jiang, M., Su, R., Wang, H., Lou, S., Fu, Q., Zhai, C., Tan, Q., Yue, D.,
896 Chen, D., Wang, Z., Xie, S., Zeng, L., Zhang, Y., 2019. Daytime atmospheric
897 oxidation capacity in four Chinese megacities during the photochemically
898 polluted season: a case study based on box model simulation, Atmos. Chem.
899 Phys. 19, 3493-3513.

900 Uttamang, P., Campbell, p., Aneja, V., Hanna, A., 2020. A multi-scale model analysis
901 of ozone formation in the Bangkok Metropolitan Region, Thailand. Atmos.
902 Environ. 229,117433.

903 Ulbrich, I., Canagaratna, MR., Zhang, Q., Worsnop, D., Jimenez, J., 2009.
904 Interpretation of organic components from positive matrix factorization of
905 aerosol mass spectrometric data. Atmos. Chem. Phys. 9, 2891–2918.

906 Warneke, C., 2004. Comparison of daytime and nighttime oxidation of biogenic and
907 anthropogenic VOCs along the New england coast in summer during New
908 england air quality study 2002. J. Geophys. Res. 109, D10309.

909 Wang, M., Lu, S., Shao, M., Zeng, L., Zheng, J., Xie, F., Lin, H., Hu, K., Lu, X.,
910 2021a. Impact of COVID-19 lockdown on ambient levels and sources of volatile
911 organic compounds (VOCs) in Nanjing, China. Sci. Total Environ. 757, 143823.
912 Wang, Y., Zhu, S., Ma, J., Shen, J., Wang, P., Wang, P., Zhang, H., 2021b. Enhanced
913 atmospheric oxidation capacity and associated ozone increases during
914 COVID-19 lockdown in the Yangtze River Delta. Sci. Total Environ. 768,
915 144796.
916 Wang, S., Yin, S., Zhang, R., Yang, L., Zhao, Q., Zhang, L., Yan, Q., Jiang, N., Tang,
917 X., 2019. Insight into the formation of secondary inorganic aerosol based on
918 high-time-resolution data during haze episodes and snowfall periods in
919 Zhengzhou, China. Sci. Total Environ. 660, 47-56.
920 Wu, F., Yu, Y., Sun, J., Zhang, J., Wang, J., Tang, G., Wang, Y., 2016. Characteristics,
921 source apportionment and reactivity of ambient volatile organic compounds at
922 Dinghu Mountain in Guangdong Province, China. Sci. Total Environ. 548-549,
923 347-359.
924 Xiong, Y., Du, K., 2020. Source-resolved attribution of ground-level ozone
925 formation potential from VOC emissions in Metropolitan Vancouver, BC. Sci.
926 Total Environ. 721, 137698.
927 Xu, Z., Huang, X., Nie, W., Chi, X., Xu, Z., Zheng, L., Sun, P., Ding, A., 2017.
928 Influence of synoptic condition and holiday effects on VOCs and ozone
929 production in the Yangtze River Delta region, China. Atmos. Environ. 168,
930 112-124.
931 Xue, L., Gu, R., Wang, T., Wang, X., Saunders, S., Blake, D., Louie, P., Luk, C.,
932 Simpson, I., Xu, Z., Wang, Z., Gao, Y., Lee, S., Mellouki, A., Wang, W., 2016.
933 Oxidative capacity and radical chemistry in the polluted atmosphere of Hong
934 Kong and Pearl River Delta region: analysis of a severe photochemical smog
935 episode. Atmos. Chem. Phys. 16, 9891-9903.
936 Yadav, R., Sahu, L., Tripathi, N., Pal, D., Beig, G., Jaaffrey, S., 2019. Investigation of
937 emission characteristics of NMVOCs over urban site of western India. Environ.

938 Pollut. 252, 245-255.
939 Yan, D., Lei, Y., Shi, Y., Zhu, Q., Li, L., Zhang, Z., 2018. Evolution of the
940 spatiotemporal pattern of $PM_{2.5}$ concentrations in China – A case study from the
941 Beijing-Tianjin-Hebei region. Atmos. Environ. 183, 225-233.
942 Yan, Y., Peng, L., Li, R., Li, Y., Li, L., Bai, H., 2017. Concentration, ozone formation
943 potential and source analysis of volatile organic compounds (VOCs) in a thermal
944 power station centralized area: A study in Shuozhou, China. Environ. Pollut.
945 223,295-304.
946 Yang, Y., Shao, M., Keßel, S., Li, Y., Lu, K., Lu, S., Williams, J., Zhang, Y., Zeng, L.,
947 Nölscher, A., Wu, Y., Wang, X., Zheng, J., 2017. How the OH reactivity affects
948 the ozone production efficiency: case studies in Beijing and Heshan, China,
949 Atmos. Chem. Phys. 17, 7127-7142.
950 Yang, Y., Liu, X., Zheng, J., Tan, Q., Feng, M., Qu, Y., An, J., Cheng, N., 2019.
951 Characteristics of one-year observation of VOCs, NOx, and O_3 at an urban site in
952 Wuhan, China. J. Environ. Sci. (in China). 79, 297-310.
953 Yang, Y., Wang, Y., Yao, D., Zhao, S., Yang, S., Ji, D., Sun, J., Wang, Y., Liu, Z., Hu,
954 B., Zhang, R., Wang, Y., 2020a. Significant decreases in the volatile organic
955 compound concentration, atmospheric oxidation capacity and photochemical
956 reactivity during the National Day holiday over a suburban site in the North
957 China Plain. Environ. Pollut. 263, 114657.
958 Yang, Y., Wang, Y., Zhou, P., Yao, D., Ji, D., Sun, J., Wang, Y., Zhao, S., Huang, W.,
959 Yang, S., Chen, D., Gao, W., Liu, Z., Hu, B., Zhang, R., Zeng, L., Ge, M., Petäjä,
960 T., Kerminen, V., Kulmala, M., Wang, Y., 2020b. Atmospheric reactivity and
961 oxidation capacity during summer at a suburban site between Beijing and Tianjin.
962 Atmos. Chem. Phys. 20, 8181-8200.
963 Yang, Y., Wang, Y., Huang, W., Yao, D., Zhao, S., Wang, Y., Wang, Y., Ji, D., Zhang,
964 R., Wang, Y., 2021. Parameterized atmospheric oxidation capacity and speciated
965 OH reactivity over a suburban site in the North China Plain: A comparative study
966 between summer and winter. Sci. Total Environ.773, 145264.
967 Yao, D., Tang, G., Wang, Y., Yang, Y., Wang, L., Chen, T., He, H., Wang, Y., 2021.

Significant contribution of spring northwest transport to volatile organic compounds in Beijing. J. Environ. Sci. (in China). 104, 169-181.

Yuan, B., Shao, M., de Gouw, J., Parrish, D., Lu, S., Wang, M., Zeng, L., Zhang, Q., Song, Y., Zhang, J., Hu, M., 2012. Volatile organic compounds (VOCs) in urban air: how chemistry affects the interpretation of positive matrix factorization (PMF) analysis. J. Geophys. Res.-Atmos. 117, D24302.

Zhang, F., Shang, X., Chen, H., Xie, G., Fu, Y., Wu, D., Sun, W., Liu, P., Zhang, C., Mu, Y., Zeng, L., Wan, M., Wang, Y., Xiao, H., Wang, G., Chen, J., 2020. Significant impact of coal combustion on VOCs emissions in winter in a North China rural site. Sci. Total Environ. 720, 137617.

Zhang, G., Xu, H., Qi, B., Du, R., Gui, K., Wang, H., Jiang, W., Liang, L., Xu, W., 2018. Characterization of atmospheric trace gases and particulate matter in Hangzhou, China. Atmos. Chem. Phys. 18, 1705-1728.

Zhang, X., Yin, Y., Wen, J., Huang, S., Han, D., Chen, X., Cheng, J., 2019. Characteristics, reactivity and source apportionment of ambient volatile organic compounds (VOCs) in a typical tourist city. Atmos. Environ. 215, 116898.

Zhang, Y., Wang, X., Zhang, Z., Lu, S., Huang, Z., Li, L., 2015. Sources of C(2)-C(4) alkenes, the most important ozone nonmethane hydrocarbon precursors in the Pearl River Delta region. Sci. Total Environ. 502, 236-245.

Zheng, H., Kong, S., Xing, X., Mao, Y., Hu, T., Ding, Y., Li, G., Liu, D., Li, S., Qi, S., 2018. Monitoring of volatile organic compounds (VOCs) from an oil and gas station in northwest China for 1 year. Atmos. Chem. Phys. 18, 4567-4595.

Zheng, H., Kong, S., Yan, Y., Chen, N., Yao, L., Liu, X., Wu, F., Cheng, Y., Niu, Z., Zheng, S., Zeng, X., Yan, Q., Wu, J., Zheng, M., Liu, D., Zhao, D., Qi, S., 2020. Compositions, sources and health risks of ambient volatile organic compounds (VOCs) at a petrochemical industrial park along the Yangtze River. Sci. Total Environ. 703, 135505.

Zheng, H., Kong, S., Chen, N., Niu, Z., Zhang, Y., Jiang, S., Yan, Y., Qi, S., 2021. Source apportionment of volatile organic compounds: Implications to reactivity, ozone formation, and secondary organic aerosol potential. Atmos. Res. 249,

105344.

Zhou, X., Li, Z., Zhang, T., Wang, F., Wang, F., Tao, Y., Zhang, X., Wang, F., Huang, J., 2019. Volatile organic compounds in a typical petrochemical industrialized valley city of northwest China based on high-resolution PTR-MS measurements: Characterization, sources and chemical effects. Sci. Total Environ. 671, 883-896.

Zhu, J., Wang, S., Wang, H., Jing, S., Lou, S., Saiz-Lopez,A., Zhou, B., 2020. Observationally constrained modeling of atmospheric oxidation capacity and photochemical reactivity in Shanghai, China. Atmos. Chem. Phys. 20, 1217-1232.

Zou, Y., Deng, X., Zhu, D., Gong, D., Wang, H., Li, F., Tan, H., Deng, T., Mai, B., Liu, X., Wang, B., 2015. Characteristics of 1 year of observational data of VOCs, NOx and O_3 at a suburban site in Guangzhou, China. Atmos. Chem. Phys. 15, 6625-6636.

Figure list:

Fig. 1 Locations of the sampling stations in Zhengzhou.

.

Fig. 2 Monthly changes in the concentrations of VOCs in Zhengzhou. The upper and lower boundaries of the boxes indicate the 75th and 25th percentiles, respectively; the lines within the boxes mark the median; the whiskers above and below the boxes indicate the 90th and 10th percentiles, respectively.

Fig. 3 Diurnal variations in VOCs compounds measured at Zhengzhou. The upper and lower boundaries of the boxes indicate the 75th and 25th percentiles, respectively; the lines within the boxes mark the median; the whiskers above and below the boxes indicate the 90th and 10th percentiles, respectively.

Fig. 4 Source profiles and contribution percentages from each source during the observation period by PMF model (bar is a mixing ratio and dot is a percentage).

Fig. 5 Conditional probability function (CPF) plots of local VOC sources in Zhengzhou. The mean (dot), median (horizontal line), 25th and 75th percentiles (lower and upper box), and 10th and 90th percentiles (lower and upper whiskers) for the entire study are shown.

Fig. 6 The contributions of each VOC source during 2018-2020.

Fig. 7 Seasonal variation of source contributions to VOCs concentration.

Fig. 8 Comparison of the relative contributions of OH, O_3 and NO_3 of the AOC in Zhengzhou during the sampling periods.

Fig. 9 Comparison of the relative contributions the OH reactivity in Zhengzhou .

Fig. 10 Top 10 VOCs species that contributed most to the Propy-Equiv and MIR weighted concentrations in Zhengzhou.

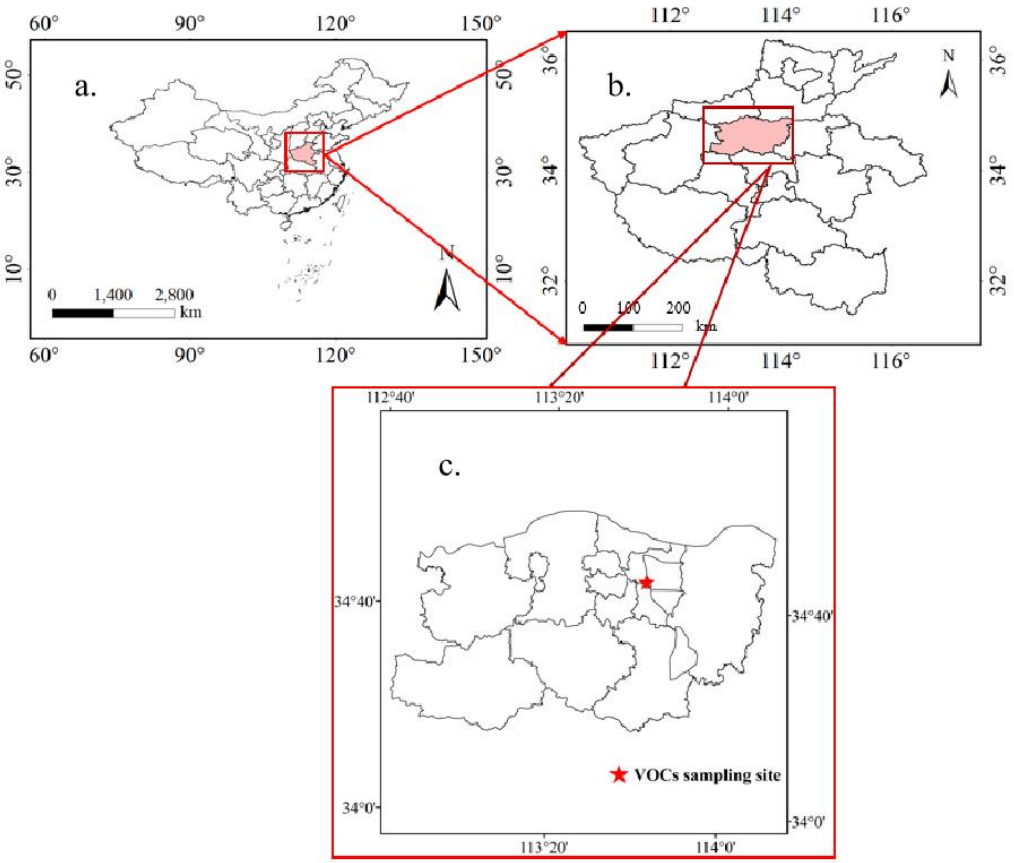

Fig. 1 Locations of the sampling stations, and Fig. a-c represents China, Henan and Zhengzhou respectively.

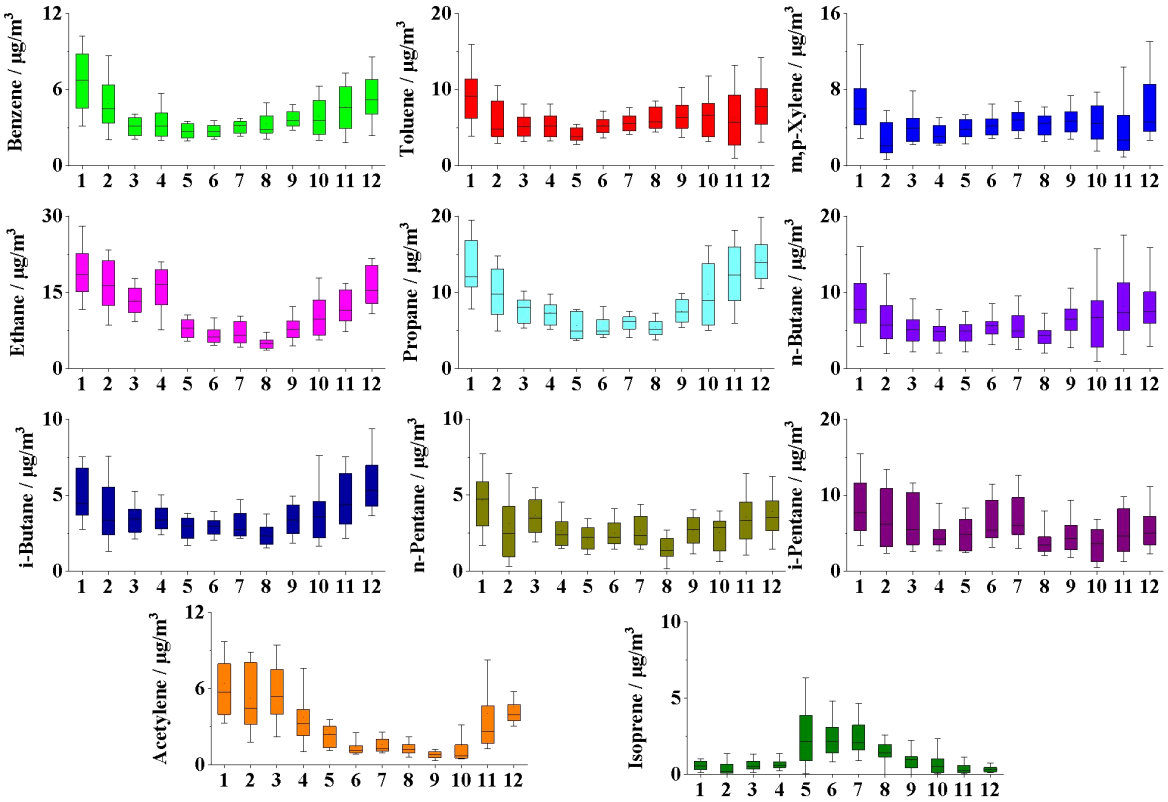

Fig. 2 Monthly changes in the concentrations of the typical VOCs species in Zhengzhou. The upper and lower boundaries of the boxes indicate the 75th and 25th percentiles, respectively; the lines within the boxes mark the median; the whiskers above and below the boxes indicate the 90th and 10th percentiles, respectively.

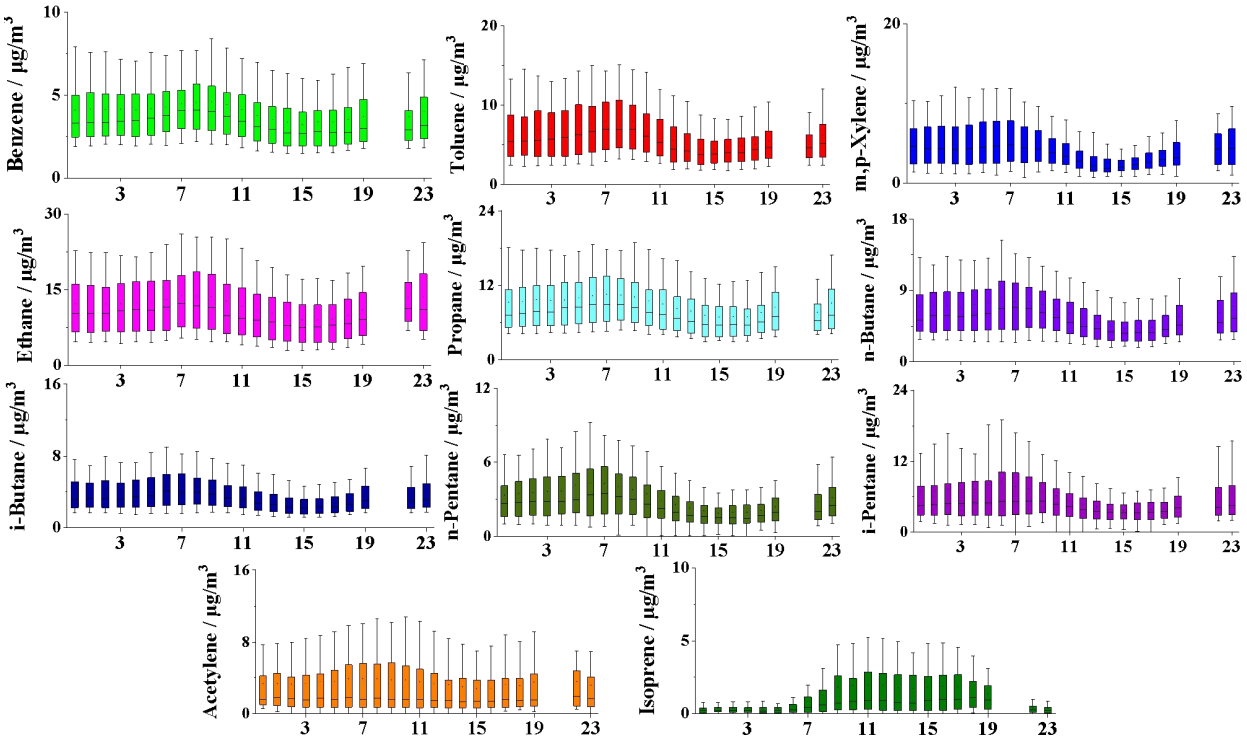

Fig. 3 Diurnal variations in VOCs compounds measured at Zhengzhou. The upper and lower boundaries of the boxes indicate the 75th and 25th percentiles, respectively; the lines within the boxes mark the median; the whiskers above and below the boxes indicate the 90th and 10th percentiles, respectively.

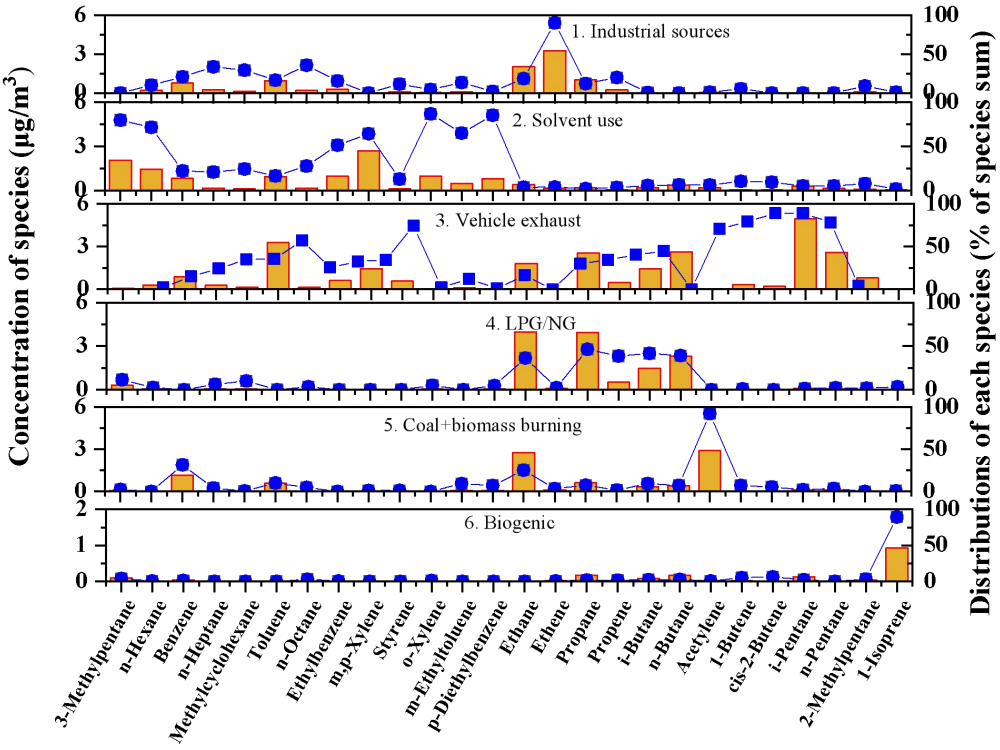

Fig.4 Source profiles and contribution percentages during the observation period by PMF model (bar is a mixing ratio and dot is a percentage).

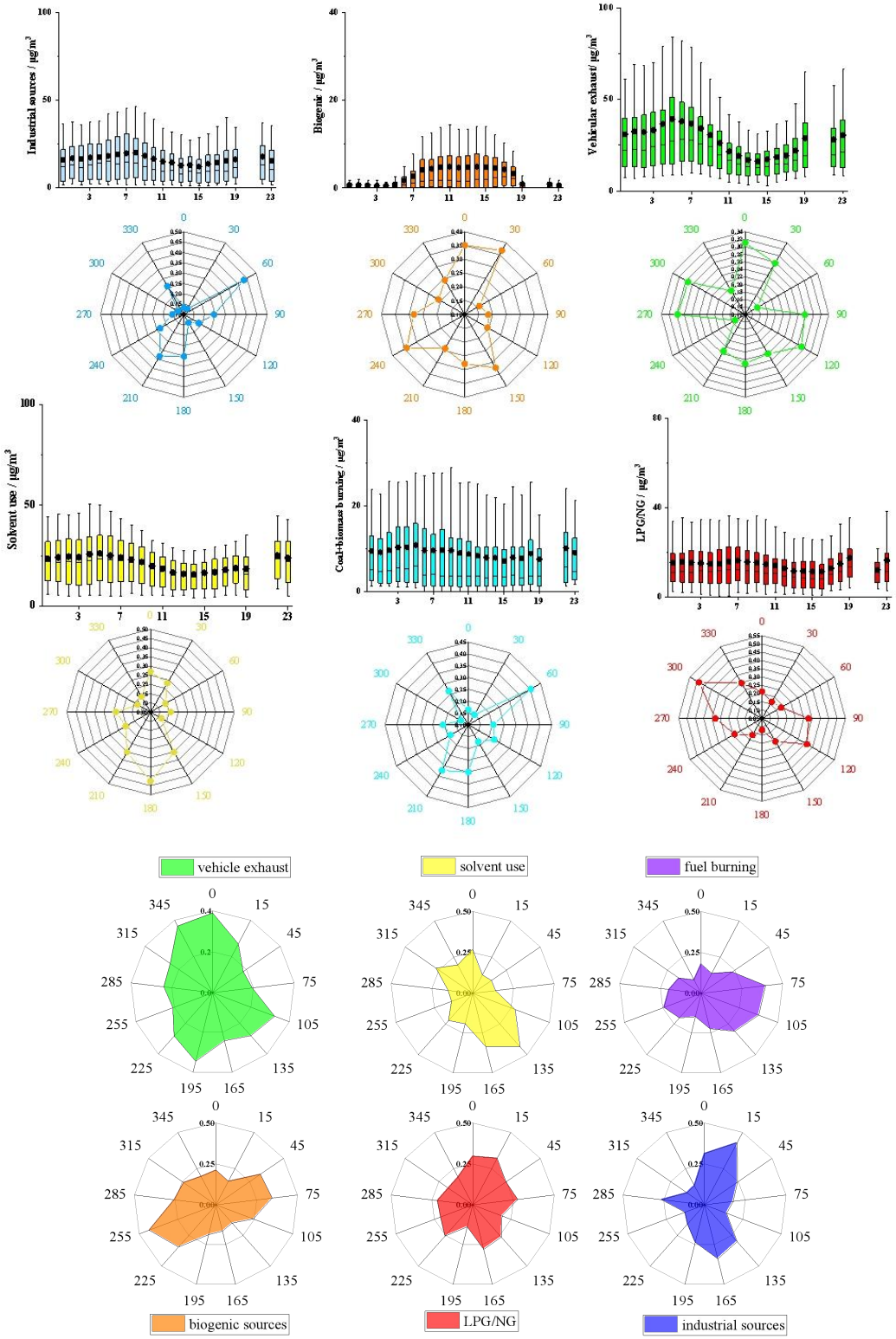

Fig. 5 Conditional probability function (CPF) plots of local VOC sources in Zhengzhou. The mean (dot), median (horizontal line), 25th and 75th percentiles (lower and upper box), and 10th and 90th percentiles (lower and upper whiskers) for the entire study are shown.

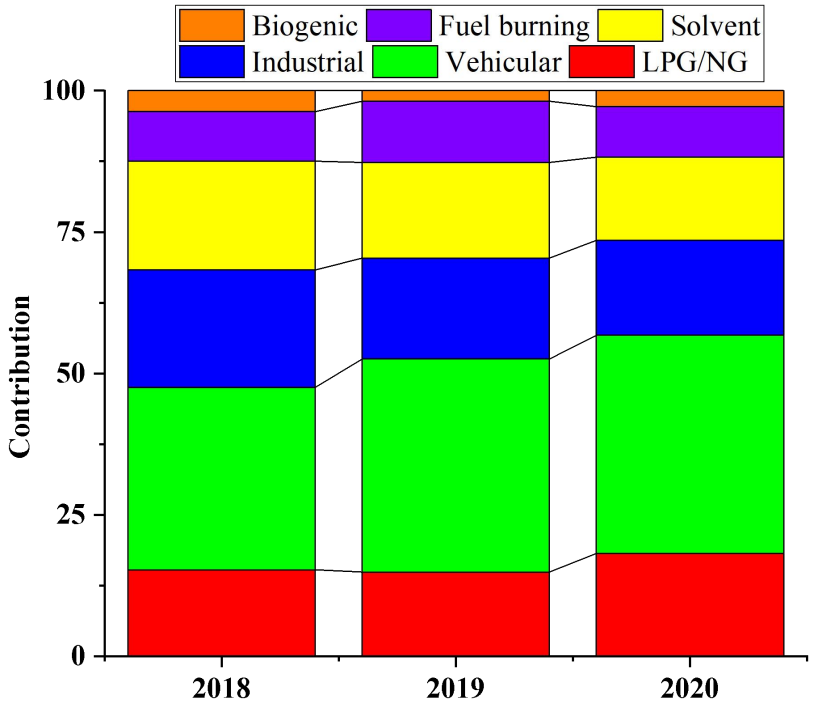

Fig. 6 The contributions of each VOC source during 2018-2020.

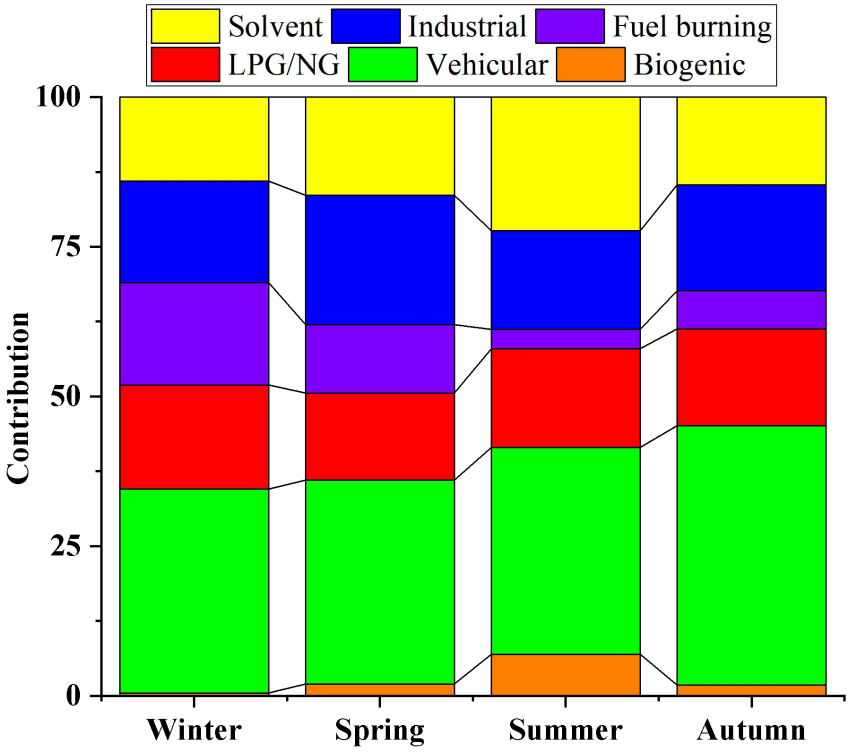

Fig. 7 Seasonal variation of source contributions to VOCs concentration.

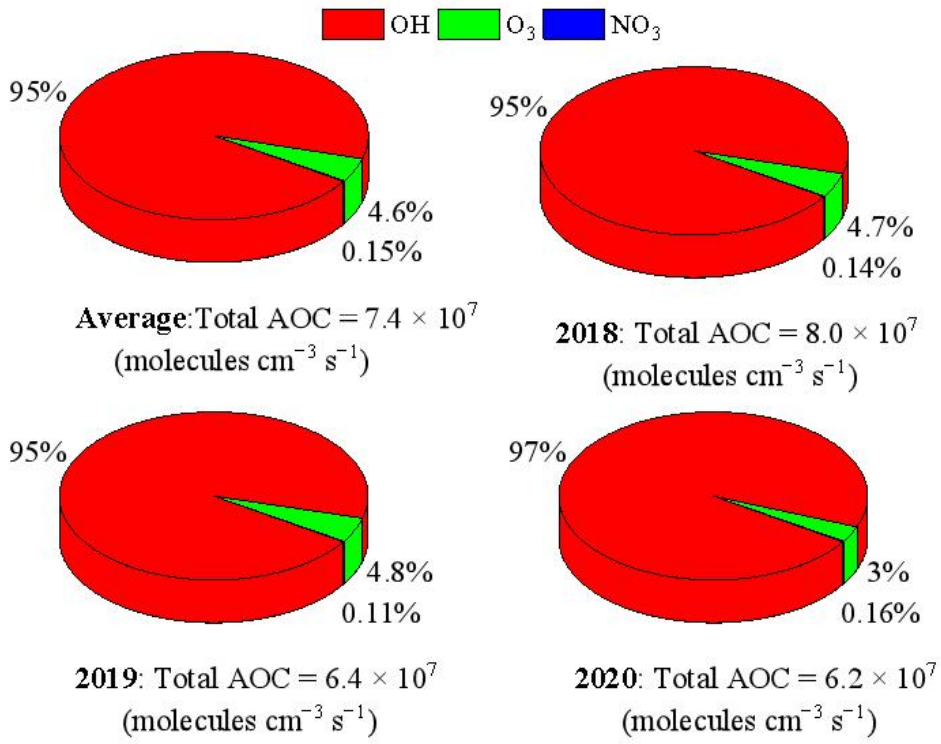

Fig. 8 Comparison of the relative contributions of OH, O_3 and NO_3 of the AOC in Zhengzhou during the sampling periods.

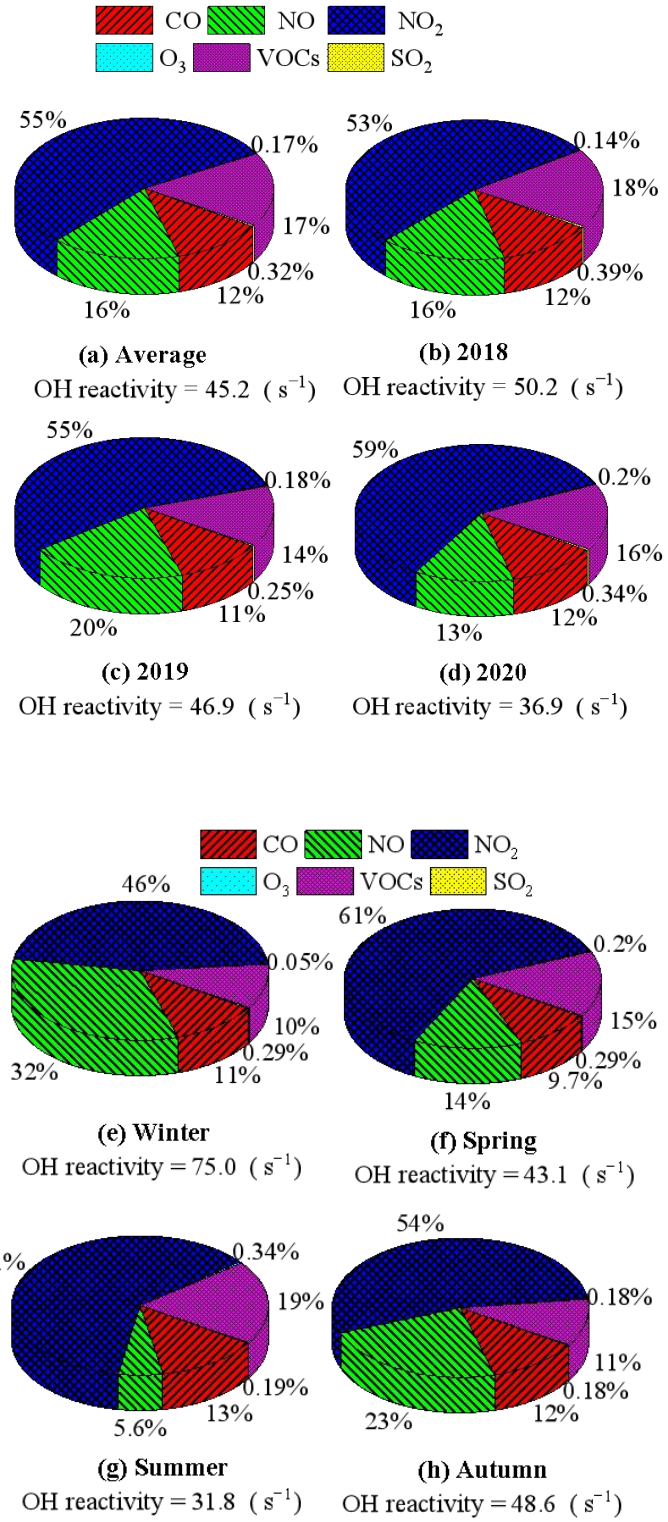

Fig. 9 Comparison of the relative contributions the OH reactivity in Zhengzhou .

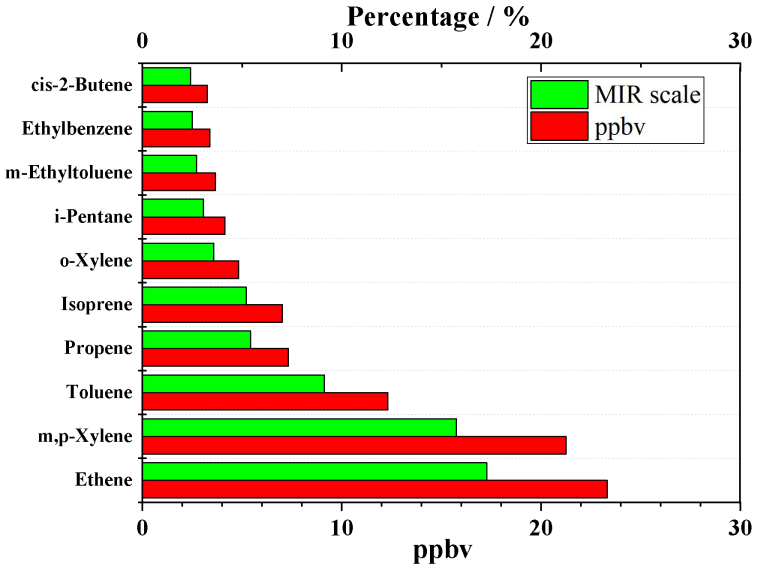

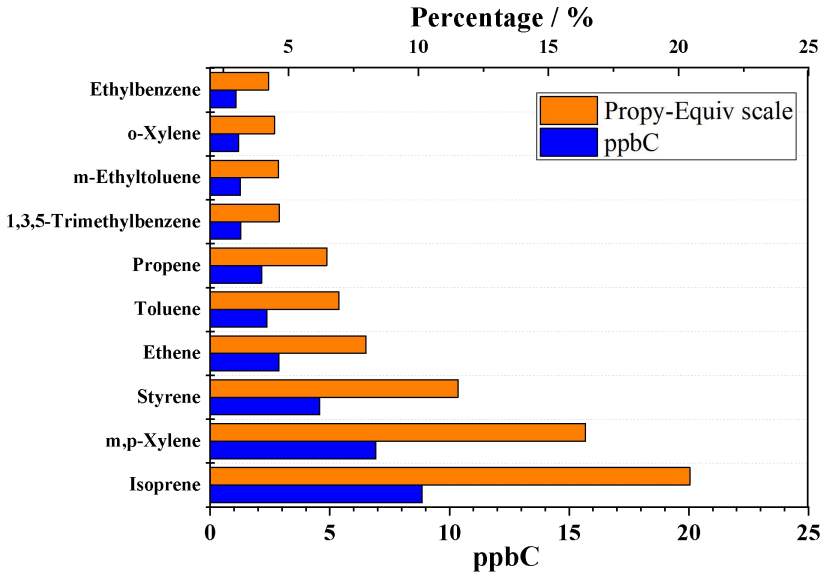

Fig. 10 Top 10 VOCs species that contributed most to the Propy-Equiv and MIR weighted concentrations in Zhengzhou.

Table list:

Table 1 Top 20 most abundant VOC species (μg/m^3) measured in Zhengzhou for the study period 2018-2020.

Table 2 Comparison of source contributions resolved by PMF models in different cities.

Table 1 Top 20 most abundant VOC species (μg/m^3) measured in Zhengzhou for the study period 2018-2020.

Species	2018	Species	2019	Species	2020	Species	Average
Ethane	13.4±7.5	Ethane	11.6±7.7	Ethane	10.2±5.3	Ethane	11.7±6.8
Propane	8.6±5.2	Propane	8.8±5.6	Propane	7.3±4	Propane	8.2±4.9
i-Pentane	7.9±19.7	n-Butane	6.2±4.7	Toluene	5.6±4.3	Toluene	6.5±4.5
Toluene	7.8±4.3	Toluene	6.1±4.7	Ethene	5.5±4.4	i-Pentane	6.1±10.4
Ethene	7.6±6.2	i-Pentane	6±6.8	n-Butane	5.4±3.7	n-Butane	5.8±4.1
n-Pentane	6±16.1	m,p-Xylene	4.5±4.4	i-Pentane	4.6±4.7	Ethene	5.6±5.3
n-Butane	5.9±3.8	Benzene	3.9±2.4	m p-Xylene	4.3±5.4	m p-Xylene	4.7±4.3
m--p-Xylene	5.2±3	Ethene	3.8±5.3	i-Butane	3.5±2.2	Benzene	3.8±2.3
Acetylene	4.9±5	i-Butane	3.8±2.7	Benzene	3.4±1.9	n-Pentane	3.8±7.3
Cyclopentane	4.4±23.4	n-Hexane	3.7±3.5	n-Pentane	2.3±2.8	i-Butane	3.5±2.4
Benzene	4.1±2.5	Acetylene	3.3±4.8	Ethylbenzene	2±2	Acetylene	3±3.6
i-Butane	3.1±2.1	n-Pentane	3.1±2.9	Isoprene	1.9±3.4	Ethylbenzene	2.4±1.8
Ethylbenzene	3.1±1.8	3-Methylpentane	2.6±1.9	n-Hexane	1.1±1.3	n-Hexane	2.2±2.2
Isoprene	2.8±3.2	Ethylbenzene	2.1±1.6	Styrene	1.1±1.7	Cyclopentane	2±9
n-Hexane	1.9±1.6	Propene	1.6±1.9	o-Xylene	1.1±1.4	1-Isoprene	1.9±2.8
o-Xylene	1.7±1	o-Xylene	1.2±1.1	Propene	1±2.2	3-Methylpentane	1.7±1.5
3-Methylpentane	1.7±1.6	2-Methylpentane	1.1±1.4	n-Heptane	1±1.6	o-Xylene	1.4±1.2
Styrene	1.6±1.2	Isoprene	1.1±1.9	m-Ethyltoluene	1±1.2	Propene	1.3±1.7
p-Diethylbenzene	1.6±1.2	Cyclopentane	1.1±2.2	n-Undecane	1±1.7	Styrene	1.2±1.3
Propene	1.4±0.9	p-Diethylbenzene	1±0.9	n-Dodecane	1±2.4	p-Diethylbenzene	1.2±1
∑TOP 20 species/∑VOCs	84%		84%		81%		83%

Table 2 Comparison of source contributions resolved by PMF models in different cities (%).

City	Sampling periods	Solvent use	Industrial sources	Vehicle exhaust	Fuel burning	LPG/ NG	Biogenic sources
Taiwan[a]	January–December 2016	29	15	18	-	-	4
Wuhan[b]	September 1, 2016 to August 31, 2017		16	24	19	13	2
Shuozhou[c]	March and August, 2014	-	14	21	30	18	-
Ningbo[d]	December 2012, April 2013, July 2013, and October 2013	7	50	16	-	27	-
Beijing[e]	March 2016 to January 2017	16	10	19	-	12	8
This study	January 2018 to December 2020	17	18	36	10	16	3

(a:Huang et al., 2019; b:Hui et al., 2018; c: Yan et al., 2017; d: Mo et al., 2017; e: Li et al., 2020c.)